FEATURE ARTICLE

A Novel Network Structure of Organometallic Clusters in the Gas Phase

Atsushi Nakajima and Koji Kaya*

Department of Chemistry, Faculty of Science and Technology, Keio University, 3-14-1 Hiyoshi, Kohoku-ku, Yokohama 223-8522, Japan, and Institute for Molecular Science, Myodaiji, Okazaki, 444-8585, Japan

Received: August 2, 1999; In Final Form: November 4, 1999

In the gas phase, novel network structures were found in organometallic clusters between metal atoms produced by laser ablation and organic ligand molecules. For 3d metal−benzene, M_nBz_m, two kinds of structures of multiple sandwich and rice-ball were formed, depending on the metal elements. Early transition metals (M_E) of Sc, Ti, and V form the multiple-decker sandwich structure of $(n, m) = (n, n + 1)$ in which metal atoms and benzene are alternately piled up, while late transition metals (M_L) of Fe, Co, and Ni form the rice-ball structure in which central metal clusters were fully covered by benzene molecules. The ionization energy of M_E−Bz drops significantly with increasing layers, which can be explained by delocalization of d electrons along the molecular axis. M−C_{60} binary clusters were also generated by a two-laser vaporization method; M_E−C_{60} clusters efficiently form a chain or a ring structure consisting of a dumbbell unit, in which metal atoms and C_{60} are alternately connected. For M_L−C_{60} clusters, however, the metal atom is tricapped by C_{60} and a face-centered tetrahedron structure is formed at $(n, m) = (4, 4)$. A similar multiple-decker sandwich structure is formed also between lanthanide metal atoms (Ln) and an organic ligand of cyclooctatetraene (COT). The Ln−COT cluster is a charge transferred cluster consisting of positively charged Ln and negatively charged COT. Their electronic structure is fairly ionic and is localized around each metal atom. These novel structures of organometallic clusters should inspire new thoughts in material science because it is hoped that the regular arrangement of metal ions can introduce useful properties such as electroconductivity and magnetism.

I. Introduction

Intrachain or multilayered organometallic polymers have been inspiring chemistry and physics for a long time.[1,2] Synthesis of organometallic compounds in gas phase presents a novel guideline to preparative chemists because they can be prepared without solvent and oxidation in air. Especially, the application of the laser vaporization to the gas-phase synthesis of organometallic compounds enables us to prepare the constituents in considerable density in a short time because there are no interfering effects of solvents, aggregation phenomena, and counterions. This new approach should open up an entirely different aspect of organometallic chemistry and physics, which can be studied quite nicely in the gas phase, and indeed several groups independently have succeeded in the synthesis of novel organometallic complexes.[3−8] The technique used to produce and detect the gas-phase organometallic clusters involves a beam source with laser vaporization of metal rods and time-of-flight mass spectrometry whose distinct ability was well-demonstrated in the discovery of C_{60}[9] and metallo-carbohedrene,[10,11] a so-called met-car.

By applying these advantages of the laser vaporization method for the metal−molecule complexes, several groups have reported gas-phase studies on metal−benzene complexes. Armentrout and co-workers[12−14] and Freiser and co-workers[15−18] have extensively reported a collision-induced dissociation (CID) experiment and have revealed thermochemistry on ML_n^+ complexes, where M and L are a metal atom and a ligand molecule, respectively. Duncan and co-workers have reported dissociation processes of metal ion−benzene complexes by laser photodissociation spectroscopy.[19−21] In their experiments, dissociative charge-transfer processes are discussed in detail. Theoretical calculations have also been carried out. In particular, Langhoff and co-workers[22] have calculated binding energies for all 3d transition metal ions (M^+) and benzene complexes and have accounted for the effect of the electron correlation between the metal atoms and benzene molecules. However, almost all the subjects were restricted to small cationic complexes denoted as $M_1(Bz)_x^+$ $(x = 1, 2)$ due to the necessity of mass selection and simplification of the calculation.

Furthermore, recently, formation of fullerene-based organometallic compounds suggests that new forms of materials can be synthesized because the fullerenes may prove to be highly versatile ligands due to their intriguing topography and aromaticity.[23−26] A great deal of effort has been spent in the past decade on modifying fullerenes by coordinating atoms both inside and outside the cage structures.[27−29] In particular, the finding of superconducting alkali metal fullerides[30−34] stimulated considerable interest, suggesting that new forms of materials and superstructures can be synthesized with important chemical and physical properties. Since C_{60} acts as not only an electron donor but also an electron acceptor, these peculiar ligand properties of C_{60} make studies of its derivatives attractive.

* Corresponding author. E-mail: kaya@ims.ac.jp.

10.1021/jp9927303 CCC: $19.00
Published on Web 12/18/1999

Interest in metal−C_{60} complexes has been driven by the potential for catalytic activity and by the possibility of forming new supermolecular compounds with new physical and chemical properties. The success of Hawkins and co-workers in forming the osmium tetraoxide derivative of C_{60}, which contains Os complexed to C_{60} through two oxygen atoms, illustrates the importance of this area of study.[35] It was through this osmylated derivative that the first X-ray structure of C_{60} was obtained.

Gas-phase studies of transition metals and C_{60} (M_T−C_{60}) have been initiated by Freiser and co-workers,[36] concerning the possibility of a transition−metal endohedral complex. Freiser and co-workers have used pulsed laser vaporization of metal and sublimation of C_{60} vapor in an FT-MS instrument and have successfully produced mass spectra of M^+−C_{60} and M^+−$(C_{60})_2$ complexes (M = V, Fe, Co, Ni, Cu, Rh, and La).[37−40] Hercules and co-worker have used argon-ion bombardment of fullerenes (C_{60} and C_{70}) deposited on a metal substrate, with the use of TOF−SIMS and have produced single metal/multifullerene adducts for Ag, Au, Rh, and Pd.[41] Through their experiments, a dumbbell structure of $M(C_{60})_2^+$ was proposed. Furthermore, Duncan and co-workers have studied the photodissociation dynamics of $Ag(C_{60})_2^+$ along with a larger aromatic ligand of coronene.[42]

For multimetal fullerene complexes in the gas phase, Martin and co-workers have extensively studied metal-coated fullerenes, where alkali metals, alkaline earth metals, and transition metals were used as metal elements.[43] In coating C_{60} and C_{70} with alkali metals, the stability of the cluster was found to be determined primarily by the electronic configuration; C_{60} with six alkali metal atoms proved to be exceptionally stable. In contrast, C_{60} and C_{70} coated by alkaline earth metals appeared with enhanced stability when the metal atoms complete metal layers on their surface. The number of alkaline earth metal atoms in the first layer is identical to the number of carbon rings; the first layer around C_{60} or C_{70} contains 32 or 37 atoms, respectively. Interestingly, the free clusters composed of single fullerene and transition metals (M = V and Ti) undergo a laser-induced transformation from metal−fullerene clusters to the met-car, M_8C_{12}.[44]

Anderson and co-workers used ion beam scattering techniques to examine interactions of transition metal cations with C_{60} over the collision energy range from 1 to 100 eV, where the metals studied are iron, manganese, chromium, molybdenum, and tungsten.[45] For each metal ion, they observed significant cross sections for electron transfer and dissociative electron transfer: At low collision energies below 15 eV, an exohedral MC_{60}^+ complex was observed without an activation barrier. Moreover, in the collision energy range of 15−40 eV, they found a second form of the MC_{60}^+ complex that is deduced as either an endhedrally bound or network bound complex. However, the system of M−C_{60} also has been restricted to either a single fullerene or single metal atom system.

As well as organometallic compounds of transition metal elements, the f-block elements of lanthanide (Ln) and actinide (Ac) metals have been of considerable importance in many areas of modern technology.[46−49] After discovery of $Ac(COT)_2$ (COT = cyclooctatetraene; C_8H_8),[50−52] studies on this criteria have extensively stimulated experimentalists and theoreticians, and $Ln(COT)_2$ were established to be trivalent complexes in bulk materials;[48,53] these findings are in agreement with theoretical calculations,[54−56] except for the case of divalent complexes of Ln = Eu and Yb. Lanthanide *p*-carbocylic complexes were synthesized as their salts of $K[Ln(COT)_2]$ by Hodgson et al., where trivalency of Ln metals overcomes aromaticity of COT^{2-}, resulting in a highly ionic complex denoted as $Ln^{3+}(COT^{1.5-})_2$. This predominantly ionic character results from the fact that the ligand of COT can act as a stable dianion, as well-known in the related actinide compounds. In the condensed phase, therefore, the alkali metal salts of $M_{alkali}^+[Ln^{3+}(COT^{2-})_2]$ are generally prepared, where positively charged M_{alkali}^+ compensates the discrepancy between 3+ oxidation states of Ln atoms and the negative charge of 4− from two COT ligands. These properties make it difficult to study neutral and multicore complexes of $Ln_n(COT)_m$, and until now, very few synthetic studies on the larger clusters have been reported except for $Ce_2(COT)_3$[57] and $[(COT)Nd(THF)_2][(COT)_2Nd]$.[58] Thus, a detailed study on the Ln−COT system is still under tardy progress. For Ln−C_{60}, a report of the superconducting $Yb_{2.5}C_{60}$ phase provides incentive for synthesizing other lanthanide C_{60} fullerides.[59] The donors of lanthanide atoms are ionized, resulting in the release of electrons to form negatively charged fullerenes.

Although these organometallic clusters have been studied extensively as mentioned above, the size range has been rather limited to small complexes. In the gas phase, recently, we have successfully found several novel network structures in organometallic clusters that were generated through the gas-phase reaction between metal atoms produced by laser ablation and organic ligand molecules.[60−69] This chapter focuses on the formation and the characterization of the superstructures composed of multimetal atoms and multiorganic ligands by use of laser vaporization, chemical probe, and photoionization methods, revealing the nature of the metal−ligand interface and their electronic structures. In these studies, 3d transition metals and lanthanide metals are used as metal elements, and Bz, C_{60}, and COT were used as organic ligand molecules.

For 3d metal−benzene, $M_n(Bz)_m$, the new organometallic compounds unknown in the bulk have been newly discovered (section III.1); two kinds of structures of multiple sandwich and rice-ball were formed, depending on the metal elements.[60−62] Early transition metals (M_E) of Sc, Ti, and V form the multiple-decker sandwich structure of $(n, m) = (n, n + 1)$,[60,62] while late transition metals (M_L) of Fe, Co, and Ni form the rice-ball structure.[61] With the measurement of the ionization energy (E_i) of M_E−Bz, it was found that the E_i drops significantly with the number of layers, which can be explained by delocalization of d electrons through the interaction with the LUMO of benzene.[70]

In the production of the 3d metal−C_{60} cluster, the technique of two independent lasers vaporizations of solid rods of vanadium and C_{60} was developed and new network structures were found (section III.2).[66] From the mass pattern of the abundant clusters and the chemical reactivity, the M_E−C_{60} clusters take chain multiple dumbbell structures,[66,68] while M_L−C_{60} clusters exhibit a tricapped structure by C_{60}, forming $M_L(C_{60})_3$.[66,70] Moreover, a face-centered tetrahedron structure is formed at $(n, m) = (4, 4)$. For Ln−COT, furthermore, we will give experimental results on the multiple-decker sandwich clusters of $Ln_n(COT)_{n+1}$ for five Ln metals of Ce, Nd, Eu, Ho, and Yb that are representative of multivalent ions such as $Ce^{3+(4+)}$, Nd^{3+}, Eu^{2+}, Ho^{3+}, and Yb^{2+}, respectively (section III.3).[68] The photoelectron spectra and size dependence of ionization energy (E_i) can reveal the ionic bonding nature, including their oxidation states. Including another structure corresponding to pyramidal Ln−C_{60} clusters (section III.4), this rich variety of newly discovered organometallic compounds will extend application of the metal atom doping to organic-ligand based materials. To obtain materials with better defined structures, it would be worthwhile to investigate the interaction

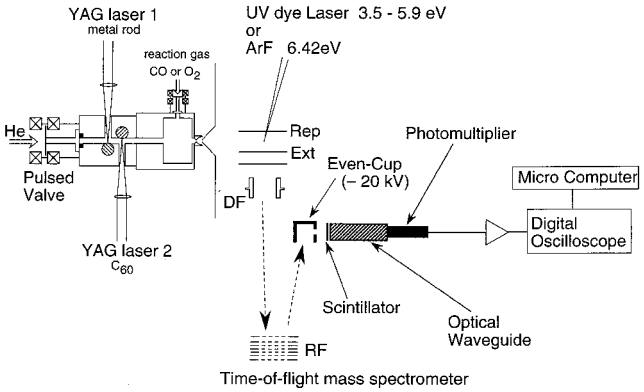

Figure 1. Schematic diagram of an experimental setup for M−C_{60} production. At the flow tube reactor, the reactant of CO or O_2 diluted by He was injected. For M−Bz or Ln−COT production, benzene or cyclooctatetraene diluted by He was injected.

of organic ligands with transition metals/lanthanides in a controlled way. Derived organometallic clusters in the gas-phase reaction will allow us to prepare well-defined deposited materials and there is much more organometallic chemistry to be explored.

II. Experimental Section

II.1. Production and Detection. *II.1.1. Metal−Benzene Clusters.* Figure 1 schematically shows an experimental setup that consists of a laser vaporization source and time-of-flight (TOF) mass spectrometer.[16,17] $M_n(Bz)_m$ clusters (M = Sc−Ni) were synthesized by the combination of a laser vaporization method and a flow-tube reactor.[72] Metal atoms were vaporized by the irradiation with the second harmonic of a pulsed Nd^{3+}:YAG laser (532 nm), and the vaporized hot metal atoms were cooled to room temperature by a pulsed He carrier gas (10 atm). Then, the metal atoms were sent into the flow-tube reactor where benzene vapor seeded in a He gas was injected in synchronization with the flowing of the metal atoms. After skimming of the cluster beam, the $M_n(Bz)_m$ clusters were ionized by an ArF excimer laser (6.42 eV) or second harmonic of a dye laser pumped by an XeCl excimer laser. The photoions were mass-analyzed by a reflectron time-of-flight (TOF) mass spectrometer, whereas the cluster cations were accelerated with a pulsed electric potential to +3 kV without photoionization. The ions were mass-analyzed by a time-of-flight (TOF) mass spectrometer with a reflectron.

II.1.2. Metal−C_{60} and Lanthanide−C_{60} Clusters. Similarly to the metal−benzene clusters, the binary clusters of both transition metal (M)−C_{60} and Ln−C_{60} were produced in the gas phase by laser vaporization; two lasers were used for metal and C_{60} rods, respectively, as shown in Figure 1. The second vaporization laser was fired with a ∼5 ms delay time after the first pulsed laser, which was adjusted to synchronize with the flow speed of the He carrier gas in order to mix them homogeneously. The fluence of the vaporization laser for the transition metal rod was 10−15 mJ/pulse, while that for the C_{60} rod was 70−100 μJ/pulse to avoid "C_2 loss" fragmentation of C_{60}. The produced hot vapors of metal and C_{60} were quenched to room temperature by a pulsed He carrier gas, and the M−C_{60} clusters were generated. The photoionized clusters were mass-analyzed by a time-of-flight (TOF) mass spectrometer with a reflectron. To detect heavy cluster ions efficiently, an ion detector known as an "even-cup" was used,[73] in which cations accelerated to 20 kV hit a cuplike aluminum dynode and the ejected electrons extracted onto a grounded scintillator were converted into photons that were detected by a photomultiplier. The C_{60} rod was prepared by pressing C_{60} powder: First, purchased C_{60} powder was uniaxially pressed into a rod of 4 mm in diameter under ∼20 MPa. Next, the roughly molded C_{60} rod was sealed into thin synthetic rubber, and after the evacuation of the air inside the rubber it was again pressed with water having pressure of ∼100 MPa This procedure effectively increases the hardness of the C_{60} rod.

II.1.3. Lanthanide−COT Clusters. Lanthanide−cyclooctatetraene complexes, $Ln_n(COT)_m$ [Ln = lanthanide metals of Ce, Nd, Eu, Ho, and Yb; COT = 1,3,5,7-cyclooctatetraene (C_8H_8)], were similarly produced by the foregoing method. Instead of benzene in the formation of metal−benzene, C_8H_8 vapor (∼70 Torr; 70 °C) diluted with He carrier gas (1.5 atm) was synchronized with the flow of the lanthanide metal vapor and was injected into the FTR, and the $Ln_n(COT)_m$ clusters were generated.

II.2. Characterization. *II.2.1. Chemical Probe and Ei Measurement.* To obtain information on the structure of $M_n(Bz)_m/M_n(C_{60})_m$, the clusters were further reacted with CO, O_2, C_2H_2, and NH_3 gas inside another flow-tube reactor, which is added downstream of the source, and their adducts produced were also mass-analyzed. In the E_i measurement for $M_n(Bz)_m/M_n(C_{60})_m/Ln_n(COT)_m$, the second harmonic of the dye laser was used as the ionization laser. The photon energy was changed at 0.01−0.03 eV intervals in the range of 5.9−3.5 eV, while the abundance and composition of the clusters were monitored by the ionization of an ArF laser. The fluences of both the tunable ultraviolet (UV) laser and the ArF laser were monitored by a pyroelectric detector (Molectron J-3) and were kept at ∼200 μJ/cm^2 to avoid multiphoton processes. To obtain photoionization efficiency curves, the ion intensities of the mass spectra ionized by the tunable UV laser were plotted as a function of photon energy with the normalization to both the laser fluence and the ion intensities of ArF ionization mass spectra. The E_i's of the clusters were determined from the final decline of the photoionization efficiency curves. The uncertainty of the E_i's is estimated to be typically ±0.05 eV.

II.2.2. Photoelectron Spectroscopy. To record photoelectron spectra, anionic complexes of $Ln_n(COT)_m$ produced by the above procedure were sent into an on-line TOF mass spectrometer at 900 eV. After being decelerated, the mass-selected anions were photodetached with the fourth harmonic (266 nm, 4.66 eV) of the other Nd^{3+}:YAG laser. The photoelectron signal was typically accumulated to 30 000 shots by a multichannel scaler/averager (Stanford Research System, SR430). An energy resolution of about 50−70 meV fwhm at 1 eV electron energy was obtained. Energy of the photoelectron was calibrated by measuring photoelectron spectra of Au^-.[74,75] The laser power for photodetachment was in the range of 1−3 mJ/cm^2 for 266 nm and no power dependent processes for the spectrum shape were observed.

III. Results and Discussion

III.1. Metal−Benzene Clusters. Parts a−h of Figure 2 show typical mass spectra of the ArF laser ionization of the $M_n(Bz)_m$ (M = 3d transition metals of Sc−Ni) clusters produced by the foregoing procedure. The features of mass spectra will be discussed in the following three parts: (1) Sc−V, (2) Cr−Mn, and (3) Fe−Ni.

III.1.1. Sc, Ti, and V. The mass spectra of early transition metals of Sc,[62] Ti,[62] and V[60] are shown in Figure 2a−c. Prominent peaks in each spectrum showed almost the same compositions, denoted as $M_n(Bz)_{n+1}$ [henceforth (n, n + 1)], although production efficiency for larger complexes depends

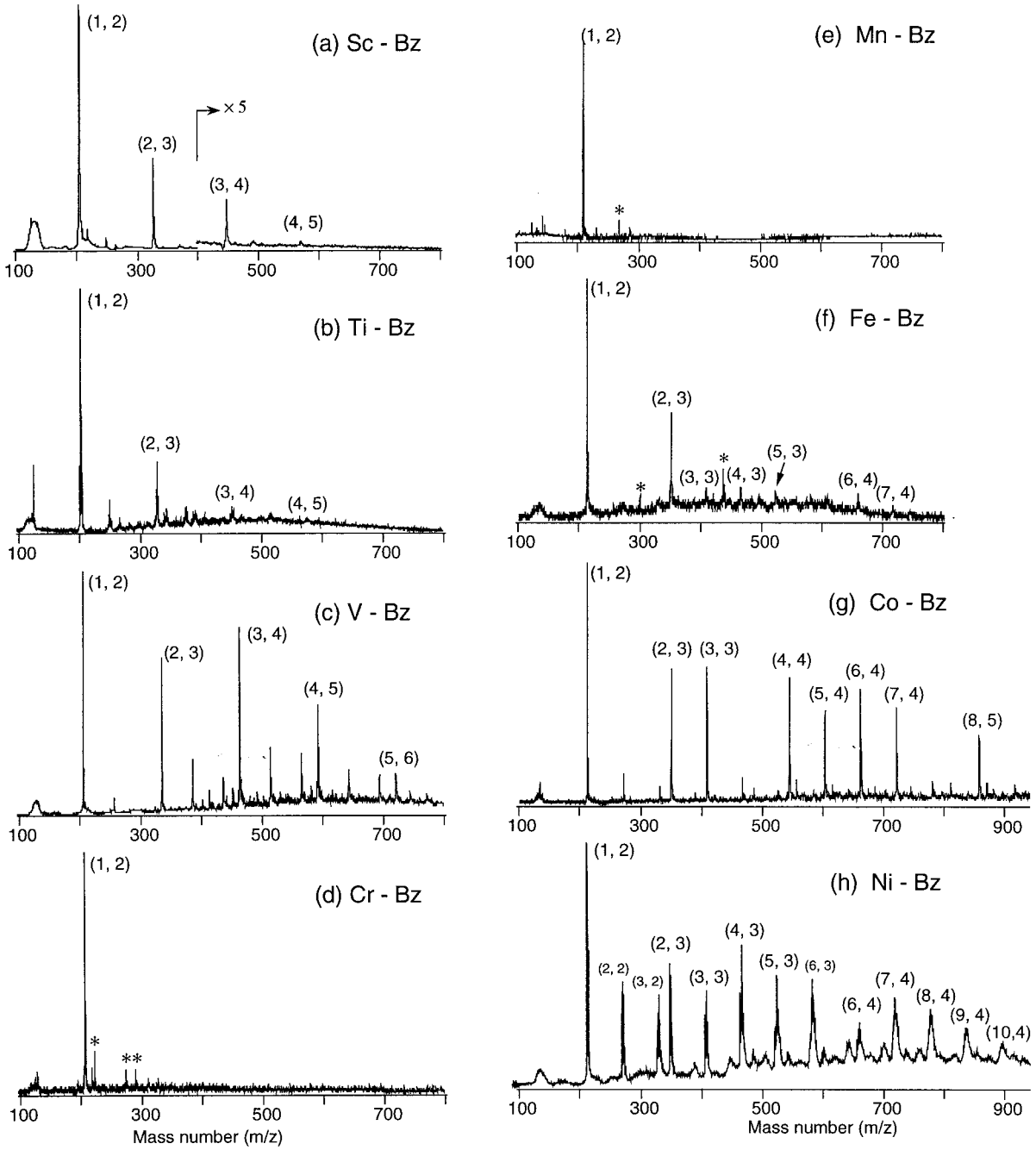

Figure 2. TOF mass spectra of the photoionized $M_n(Bz)_m$ clusters by the ArF laser (M = 3d transition metals): (a) Sc−Bz; (b) Ti−Bz; (c) V−Bz; (d) Cr−Bz; (e) Mn−Bz; (f) Fe−Bz; (g) Co−Bz; (h) Ni−Bz.

on the metal elements. These prominent peaks of (n, $n + 1$) remained unchanged in the mass spectrum, even if (1) the concentration of benzene vapor was changed to a higher one and (2) the CO reactant was exposed additionally. This result indicates that all the metal atoms of (n, $n + 1$) are contained as an inner component, because an exterior metal atom should result in a site of CO adsorption. Furthermore, when the concentration of metal vapor was changed to a higher value, new minor peaks denoted as (n, n) and ($n + 1$, n) appeared in the spectrum, but no peaks for ($n + 2$, n). These two kinds of additional clusters showed adsorption reactions toward CO, resulting in (n, n) + 3CO and ($n + 1$, n) + 6CO for V−Bz. These results on mass spectra in the chemical probe experiment indicate that the $M_n(Bz)_{n+1}$ clusters are sandwich clusters in which metal atoms and benzene molecules are alternately piled up. Namely, the superfluous metal atom(s) over the (n, $n + 1$) composition are exterior atoms and are placed at the terminal of clusters up to two atoms. These (n, n) and ($n + 1$, n) clusters reasonably correspond to a sandwich cluster having one and two exterior metal atom(s), respectively. Because there are two sites for the exterior atoms, the ($n + 2$, n) cluster is missing. This result of the chemical probe experiment leads us to conclude that the most explicable structure for $Sc_n(Bz)_m$, $Ti_n(Bz)_m$, and $V_n(Bz)_m$ clusters is a multiple-decker structure (Figure 3a).[60,62] Very recently, indeed, Bowers and co-workers did an ion mobility experiment for the $V_n(Bz)_m$ clusters and reported that they really take the multiple sandwich structure.[76] They also found that the mass-selected V_n^+ clusters ($n = 4$) form the sandwich clusters of $V_n(Bz)_{n+1}^+$ through the reaction with benzene molecules, indicating major reorganization occurs when benzene interacts with the vanadium cluster. This finding

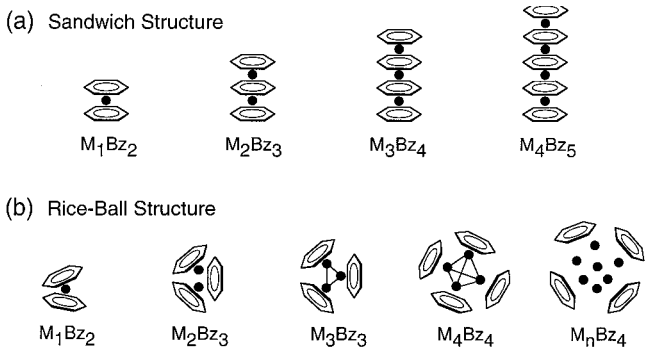

Figure 3. (a) Proposed structures for early transition metals for Sc, Ti, and V; a multiple sandwich structure. (b) Proposed structures for late transition metals for Fe, Co, and Ni; a rice-ball structure.

TABLE 1: Ionization Energy (E_i) of $M_n(C_{60})_m(Bz)_k$ Clusters (M = Sc, Ti, V, and Cr) in eV

	ionization energy			
cluster	M = Sc	M = Ti	M = V	M = Cr
$M_1(Bz)_2$	5.05(5)	5.68(4)	5.75(3)	5.43(2)
$M_2(Bz)_3$	4.30(5)	4.53(5)	4.70(4)	
$M_3(Bz)_4$	3.83(5)	4.26(5)	4.14(5)	
$M_1(C_{60})_1(Bz)_1$	5.54(3)		5.61(3)	5.71(3)
$M_1(C_{60})_1$	5.92−6.42	5.92−6.42	5.92−6.42	5.92−6.42
$M_1(C_{60})_2$	5.75(5)[a]	5.93(5)	5.82(5)	5.67(3)
$M_1(C_{60})_3$				5.71(5)
$M_2(C_{60})_3$	5.92−6.42		5.92−6.42	
$M_3(C_{60})_4$	5.92−6.42		5.92−6.42	

[a] 5.75(5) represents 5.75 ± 0.05.

is ascribed to the large stability of sandwich clusters V−Bz through d−π interaction.

E_i's of $Sc_n(Bz)_m$, $Ti_n(Bz)_m$, and $V_n(Bz)_m$ clusters were measured by the photoionization method, and the E_i values are tabulated in Table 1.[60,62] Figure 4a shows the E_i values plotted against the number of metal atoms. The E_i values drastically decrease with cluster size n, although the clusters consist of metal atoms and benzenes having relatively high E_i's; E_i(Sc) = 6.54 eV, E_i(Ti) = 6.82 eV, E_i(V) = 6.74 eV, and E_i(Bz) = 9.24 eV.[77] The trend of the E_i decrement is understood as a common feature for the multiple-decker sandwich structure. This phenomenon of E_i decrement has been theoretically elucidated by ab initio calculations, showing that the ionization occurs from the delocalized molecular orbital of metal−metal interaction interposed by π^* orbitals of benzene.[70] Along the molecular axis of the sandwich cluster, one-dimensional delocalization of the metal dδ(e_{2g}) orbitals occurs through the LUMO (e_{2g}) of C_6H_6, giving a drastic decrement of E_i.

III.1.2. Cr and Mn. In the case of Cr and Mn, only the (1, 2) complex was produced (Figure 2d,e). The structure of these clusters is reasonably concluded to be a sandwich structure, as reported in bulk synthesis of $Cr_1(Bz)_2$. It should be noted that the peak intensity of $Cr_1(Bz)_2$ and $Mn_1(Bz)_2$ was relatively small and was estimated to be about 1/10 and 1/200 of $V_1(Bz)_2$ under similar production conditions, respectively. In contrast to the mass spectra of Sc−, Ti−, and V−benzene, the characteristic distribution implying the multiple sandwich structure vanished in the mass spectra of Cr− and Mn−Bz. As reported elsewhere,[65] the poor distribution in larger cluster sizes is explicable by electron spin restriction in a growth process. On the assumption of the electron spin conservation, multiple step nonadiabatic transitions are required to produce the Cr− and Mn−benzene complexes, because the metal−benzene complexes generally prefer to have lower electron spin states in contrast to the high electron spin state of the ground state of Cr and Mn atoms. The large difference of electron spin between the complexes and the reactant metal atoms is attributed to the poor production of larger clusters.

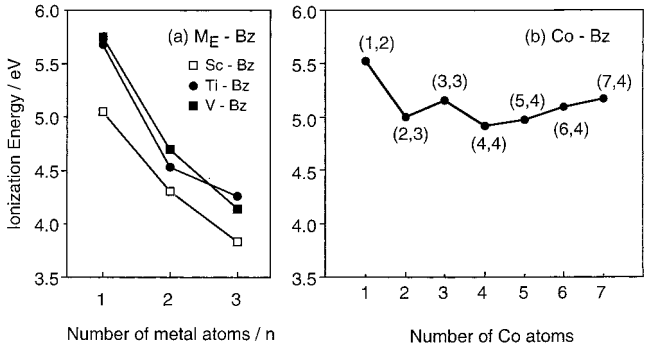

Figure 4. Ionization energies of (a) $Sc_n(Bz)_m$, $Ti_n(Bz)_m$, and $V_n(Bz)_m$ clusters and (b) $Co_n(Bz)_m$ plotted against the number of metal atoms from n = 1 to 3: (□) E_i's of $Sc_n(Bz)_{n+1}$; (●) E_i's of $Ti_n(Bz)_{n+1}$; (■) E_i's of $V_n(Bz)_{n+1}$. For M_E−Bz, they decrease rapidly with the number of layers, while for M_L−Bz they change gradually with the cluster size.

III.1.3. Fe, Co, and Ni. Late transition metal−benzene complexes of Fe, Co,[61] and Ni were also produced. Parts f−h of Figure 2 show the mass spectra of $M_n(Bz)_m$ clusters under a relatively high concentration of benzene vapor. Even if the concentration of benzene was changed to a higher one, the mass spectrum remained unchanged. Therefore, $M_n(Bz)_m$ clusters exhibit the specific maximum m value (m_{max}) for each n. This behavior in the mass spectrum is completely different from that of the multiple-decker sandwich clusters.

When the magic-number clusters having m_{max} were exposed to NH_3 reactant gas, all of them were unreactive. In contrast to this, other small mass peaks, such as (n, m) = (1, 1), (2, 2), (3, 2), and (4, 3), are depleted completely by the reaction with NH_3, and instead, mass peaks corresponding to the adduct of $Co_n(Bz)_mNH_3$ newly appear in the spectrum. Since it is known that one NH_3 molecule is adsorbed onto one Co atom,[78] this result implies that all of the magic-number clusters have no exterior Co atoms and that the less abundant clusters of (1, 1), (2, 2), (3, 2), and (4, 3) have one exterior Co atom. Namely, the magic-number clusters are saturatedly covered with benzene molecules, and no NH_3 molecule interacts with Co atoms in the clusters. The magic-number behavior of $Co_n(Bz)_m$ cannot be explained only by the sandwich structure, because the sandwich clusters having formulas of (3, 3), (4, 4), and so on, should have an exterior Co atom that is expected to be a reactive site toward NH_3. Taking into account the two facts that every number of Co atoms (n) has a specific m_{max} and that they have no exterior Co atoms, the most plausible structure of $Co_n(Bz)_m$ is the structure of Co_n clusters covered with benzene molecules (m); a rice-ball structure with sea laver as shown in Figure 3b.

For Ni, the mass spectrum of $Ni_n(Bz)_m$ clusters was shown in Figure 2h, where the Ni_n cluster occasionally takes two numbers of benzenes even under a saturation condition at n = 2, 3, 6, and 10. At n = 2, for example, both the (2, 2) and (2, 3) peaks were observed, and their intensity ratio was almost constant with a higher concentration of benzene. Although there is ambiguity of m_{max}, the numbers of benzene for each n are similar to those of $Co_n(Bz)_m$. Thus, this behavior seems to indicate these observed $Ni_n(Bz)_m$ clusters also take the structures of Ni_n clusters fully surrounded by benzene molecules. In the case of $Fe_n(Bz)_m$, peaks denoted as (1, 2) and (2, 3) were mainly observed together with weak peaks of (3, 3), (4, 3), (5, 3), (6, 4), and (7, 4). Similar to the case of Co and Ni, the peaks of n

TABLE 2: Comparison of Total Valence Electrons of $Co_n(Bz)_m$ and $Co_n(CO)_m^+$ Clusters

$Co_n(CO)_m^+ = (n, m)^a$	total VEs	$Co_n(Bz)_m = (n, m)$	total VEs
(2, 8)	33	(2, 3)	36
(3, 10)	46	(3, 3)	45
(4, 12)	59	(4, 4)	60
(5, 14)	72	(5, 4)	69
(6, 16)	85	(6, 4)	78
(7, 19)	100	(7, 4)	87
(8, 20)	111	(8, 5)	102

[a] Reference 79.

= 3 seem to be a structure fully covered by benzene molecules, taking the rice-ball structure.

In this rice-ball structure, m_{max} should be governed by an electronic and/or a geometric factor. For a multinuclear system, reactions of metal clusters with CO provide profitable information on the electronic stability of the clusters,[79−81] in which a mass-selected metal cluster is reacted with CO molecules as many as it can take up. The number of adsorbed CO molecules thus obtained directly reflects the maximum number of VEs that can fill in the valence orbital of the complex, because CO molecules lead to little steric hindrance between each other. By comparing the number of VEs of carbonyl and benzene clusters, the stability of $M_n(Bz)_m$ clusters can be discussed from an electronic point of view. According to Castleman and co-workers,[79] each Co_n^+ cluster has a maximum number of CO molecules for adsorption. By considering CO and the benzene ligand as a two- and six-electron donor together with the nine d electrons of the Co atom, valence electrons of neutral $Co_n(CO)_m$ and $Co_n(Bz)_m$ can be counted as listed in Table 2. As cluster size n increases, the observed number of benzene addition starts to become less than the expected one. That is to say, the observed $Co_n(Bz)_m$ clusters do not necessarily follow the electronic demand of the metal clusters. For Ni clusters,[80,81] the same deviation from the expected number of benzene molecules is also seen at large n. These results indicate that, with increasing cluster size, m_{max} is governed not only by an electronic structure but also by a geometry of corresponding metal cluster (M_n). It is reasonable that the number of benzene molecules is restricted by a geometrical factor because steric hindrance between benzene molecules becomes crucial at large n. E_i's of $Co_n(Bz)_m$ were also measured by the photoionization method, as shown in Figure 4b. The E_i's of $Co_n(Bz)_m$ increase at $n = 4$, and the E_i dependence of the cluster size is in contrast to those of $V_n(Bz)_m$. This result is attributed to the difference in their structures: the sandwich clusters for V and the rice-ball structure for Co. Indeed, the E_i difference between (6, 4) and Co_6 or between (7, 4) and Co_7 is less than 1 eV,[82] which suggests that they have a common framework of the Co_n cluster.

III.1.4. Formation Mechanism. Two mechanisms are possible for the production of the M−Bz clusters. They are (a) benzene molecules reacted with metal clusters, and (b) benzene molecules sequentially reacted with metal atoms. It is meaningful to discuss the difference of the formation mechanisms of $Co_n(Bz)_m$ and $V_n(Bz)_m$ from the viewpoint of the reactivity of cationic Co_n^+ and V_n^+ clusters. As studied by Zakin et al.,[83] sequential dehydrogenation channels for $V_nC_6H_k^+$ ($k = 5$) have been observed in the reaction with the V_n^+ clusters toward C_6D_6; the reaction of the cluster proceeds via facile initial chemisorption followed by activated C−D cleavage and D_2 elimination. Therefore, mechanism b should be the main route of the sandwich clusters of $V_n(Bz)_m$, because no dehydrogenated species were observed in the present work of the sandwich cluster. The reaction products of the V_n clusters with benzene could not be observed in the mass spectrum, probably because the products were distributed over the wide range of the compositions of $V_nC_mH_k$ under high concentrations of benzene. As mentioned above, however, Bowers and co-workers have pointed out that the V_n cluster can contribute to the formation of the sandwich V−Bz clusters,[76] so that the formation mechanism should seemingly be examined more closely.

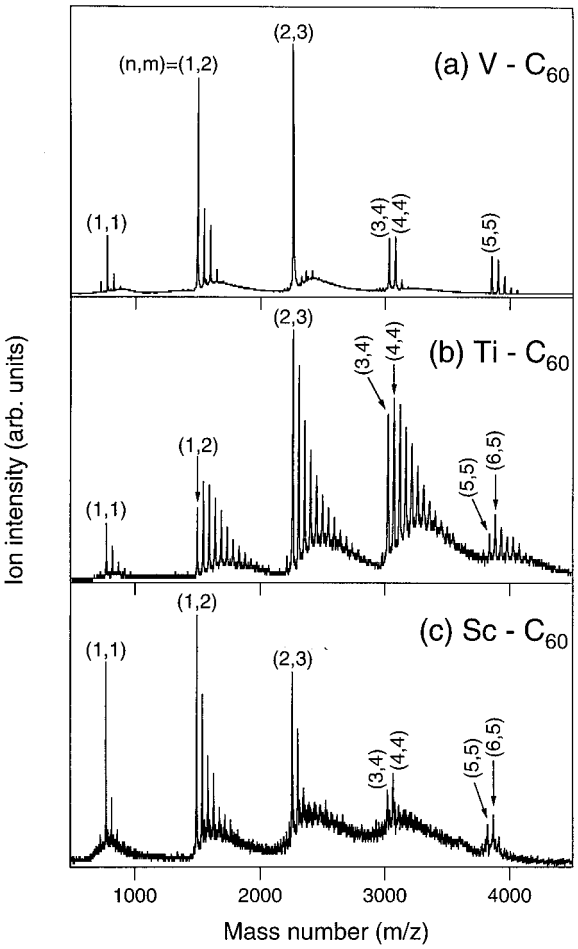

Figure 5. TOF mass spectra of transition metal (M = Sc, Ti, and V)−C_{60} cations, $M_n(C_{60})_m^+$: (a) $Sc_n(C_{60})_m^+$; (b) $Ti_n(C_{60})_m^+$; (c) $V_n(C_{60})_m^+$. Peaks of the clusters are labeled according to the notations (n, m), denoting the number of metal atoms (n), C_{60} molecules (m).

On the other hand, the reactivity study of Co_n^+ clusters toward benzene has been reported by Irion et al.[84] According to their result, the Co_n^+ cluster reacts with benzene, forming their adduct without dehydrogenation. Then, it is deduced that the reacted Co_n clusters with benzene could be observed clearly, because the products were stacked at the specific compositions of $Co_n(Bz)_{mmax}$ under high concentrations of benzene. In fact, the cluster rich condition was essential to produce the large $Co_n(Bz)_m$ clusters. Thus, mechanism a can contribute to the formation of the $Co_n(Bz)_m$ cluster.

III.2. Metal-C_{60} Clusters. *III.2.1. Structures of Sc−C_{60}, Ti−C_{60}, and V−C_{60} Clusters.* Figure 5 shows TOF mass spectra of $M_n(C_{60})_m^+$ (M = (a) Sc, (b) Ti, and (c) V) cluster cations, which were directly extracted from the beam without photoionization.[66,68] Peaks of the cationic clusters are labeled according to the notation $(n, m)^+$, denoting the number of metal atoms (n) and C_{60} (m). Under this condition, the contribution of M_n^+ cluster to $M_n(C_{60})_m^+$ formation was negligible because the abundance of the M_n^+ clusters ($n = 2$) was less than 1/100 compared to that of the M^+ atom. The mass spectrum of $Ti_n(C_{60})_m^+$ was obtained with higher laser fluence for metal

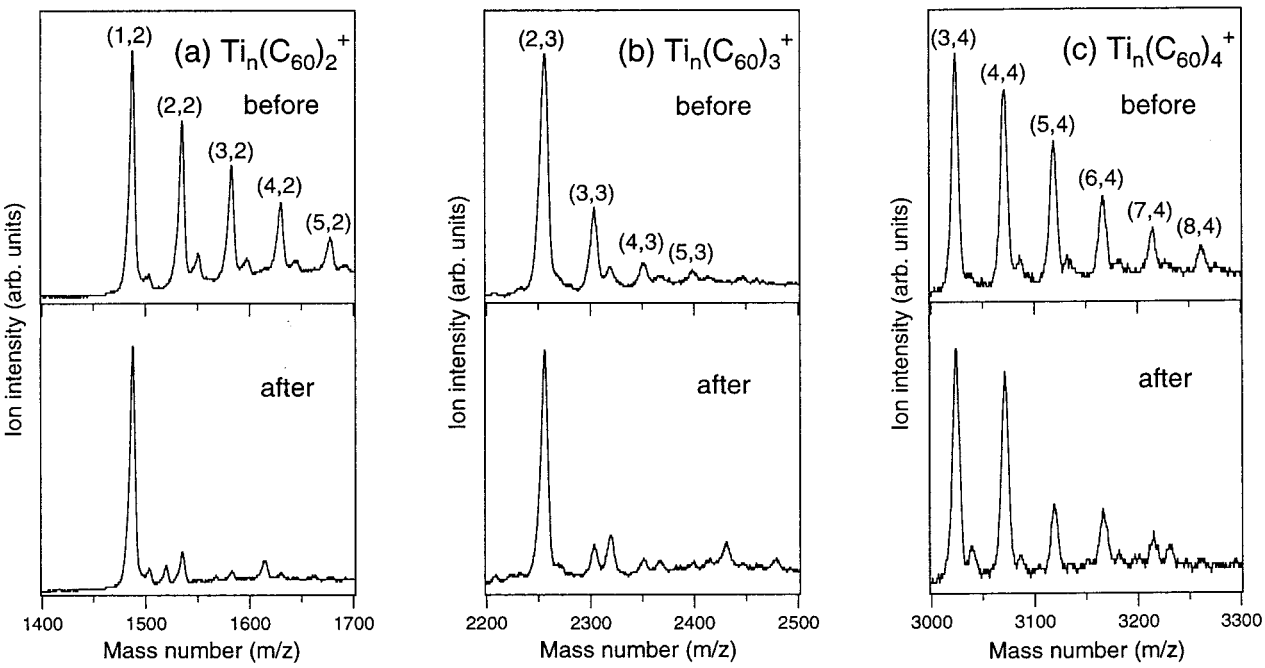

Figure 6. Expanded view of time-of-flight mass spectra of before (top) and after (bottom) oxidation reactions: (a) $Ti_n(C_{60})_2^+$; (b) $Ti_n(C_{60})_2^+$; (c) $Ti_n(C_{60})_4^+$.

vaporization compared with the others. As a result, the clusters having rich metal atoms were formed abundantly. These TOF mass spectra indicate three common features: (i) main products are $(1, 2)^+$, $(2, 3)^+$, $(3, 4)^+$, $(4, 4)^+$, and $(5, 5)^+$, (ii) $(4, 4)^+$ is more abundant than $(3, 4)^+$, while $(5, 4)^+$ is less abundant than $(4, 4)^+$, and (iii) $(4, 5)^+$ is scarcely produced (instead, $(5, 5)^+$ is the first prominent peak in the $(n, 5)^+$ series).

To deduce the structure of the M−C_{60} clusters by the chemical probe method, the reactivity of these abundant clusters toward O_2 gas was measured. Figure 6 shows mass spectra of $Ti_n(C_{60})_m^+$, before and after the oxidation reaction. The abundant clusters with $(n, m) = (1, 2)^+$, $(2, 3)^+$, $(3, 4)^+$, $(4, 4)^+$, and $(5, 5)^+$ were nonreactive toward O_2, whereas the other species drastically diminished with the injection of O_2, followed by O atom adduct formation ($Ti_n(C_{60})_mO_k^+$). It is reasonably presumed that an exterior Ti atom in $Ti_n(C_{60})_m^+$ is a reaction site to the oxidation, because C_{60}^+ itself does not show the oxidation reaction. Namely, these results indicate that the Ti−C_{60} clusters of $(1, 2)^+$, $(2, 3)^+$, $(3, 4)^+$, $(4, 4)^+$, and $(5, 5)^+$ have no exterior Ti atoms. As well as the Ti−C_{60} clusters, the abundant species of the Sc−C_{60} and the V−C_{60} clusters also show no reactivity toward O_2. On the basis of no reactivities toward O_2 or CO gas, therefore, the presumed geometry of $(n, n + 1)^+$ at $n =$ 1−3 is a multiple dumbbell structure (Figure 8a−c) and that of $(n, n)^+$ at $n = 4$−5 is a ring structure (Figure 8d−e) where the metal atom and C_{60} are alternatively piled up. There is no necessity for assuming linear chain structures of $(n, n + 1)^+$ at $n = 2$ and 3, because C_{60} consists of many rings for bonding sites; 12 pentagonal rings and 20 hexagonal rings. Very recently, Martin and co-workers independently reported a similar network structure for polymerized C_{60} linked by carbon atoms. Carbon atoms also act as bonding elements between fullerenes, resulting in the formation of polymers $C_{60}(CC_{60})_{n-1}$.[85]

We obtained the TOF mass spectra of neutral $M_n(C_{60})_m$ clusters by the use of an ArF laser, whose features are identical with those of $M_n(C_{60})_m^+$ cluster cations. Then, it is reasonably presumed that $(n, m) = (1, 2)$, $(2, 3)$, $(3, 4)$, $(4, 4)$, and $(5, 5)$ for the neutral $M_n(C_{60})_m$ clusters also have the dumbbell or the ring structures. Experimentally it was relatively difficult to obtain the mass spectra of the neutral $M_n(C_{60})_m$ clusters by the photoionization compared to those of the $M_n(C_{60})_m^+$ cluster cations, because of their low ionization efficiencies. This is probably because their ionization energy is close to the photon energy of the ArF laser (6.42 eV), which will be discussed below in section 3.2.5.

III.2.2. Reactivity of $M_n(C_{60})_m^+$ (M = Sc, Ti, and V) Cluster Cations toward CO. To investigate the metal−C_{60} bonding in the dumbbell clusters, the examination of the reactivity of $M_n(C_{60})_m^+$ (M = Sc, Ti, and V) toward CO gas was performed.[66,68] Since CO can generally be regarded as a two-electron donor, the determination of the maximum number of CO adsorption (k_{max}) enables us to apply electron counting to the complexes. The metal atom in $M_n(C_{60})_m^+$ is a reaction site to the CO reaction because C_{60}^+ itself is inert for CO as well as O_2. The reactivity measurement indicates that the abundant dumbbell/ring clusters were nonreactive, whereas the other $M_n(C_{60})_m^+$ clusters reacted with CO, forming carbonyl complexes. In the mass spectra of $Sc_n(C_{60})_1^+$ before and after the reaction with CO, $Sc_1(C_{60})_1^+$ decreases clearly, and instead, $Sc_1(C_{60})_1(CO)_4^+$ appears newly. Even with a higher concentration of CO, $Sc_1(C_{60})_1(CO)_4^+$ is produced as a final product of $Sc_1(C_{60})_1^+$ and therefore k_{max} is 4 for $Sc_1(C_{60})_1^+$. On the other hand. $Ti_1(C_{60})_1^+$ and $V_1(C_{60})_1^+$ resulted in $Ti_1(C_{60})_1(CO)_3^+$ and $V_1(C_{60})_1(CO)_3^+$, respectively, and their k_{max} is 3.

For organometallic complexes, the 18-electron rule is useful to discuss their electronic stability qualitatively.[86] Armentrout and co-workers have reported that $V(CO)_n^+$ and $Ti(CO)_n^+$ are formed up to $n = 7$, satisfying the 18-electron rule strictly.[87,88] However, the dissociation energies of $V(CO)_{n-1}^+$−CO and those of $Ti(CO)_{n-1}^+$−CO at $n = 7$ are about half the value of those at $n = 4$−6, suggesting that the satisfaction of 16 valence electrons (VEs) can make the clusters stable toward CO addition.[87,88] On a MO diagram under C_{6v} or D_{6h} symmetry, indeed, the ninth orbital filled by the 17th and 18th electrons has nonbonding character, leading to less electronic stabilization.[89] In fact, almost no $Ti(CO)_7^+$ and $V(CO)_7^+$ was observed under our conditions, while $Ti(CO)_6^+$ and $V(CO)_6^+$ were abundantly produced. Total numbers of VEs of $Ti(CO)_6^+$ and

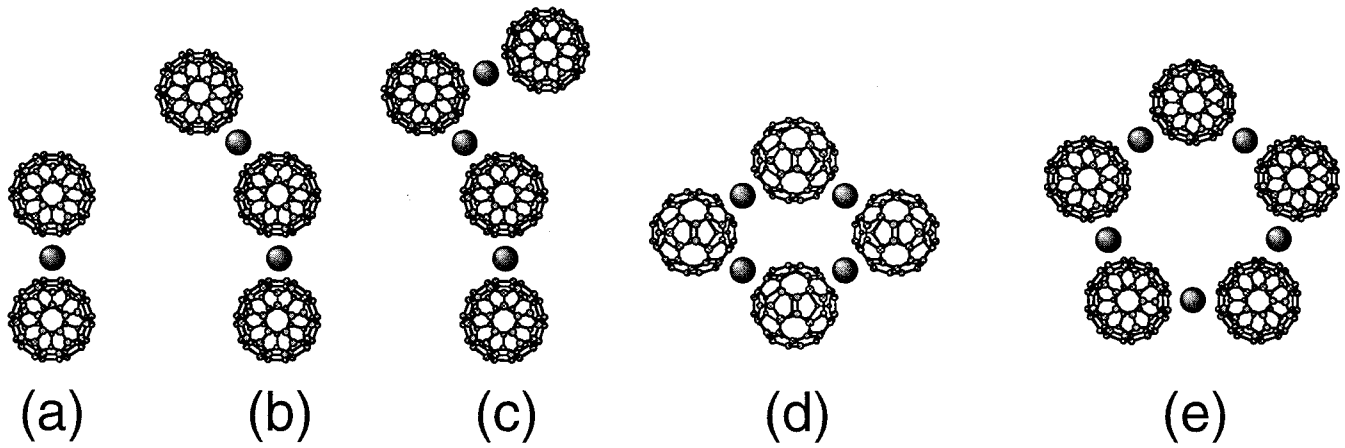

Figure 7. Proposed geometric structures of (a) $M_1(C_{60})_2^+$, (b) $M_2(C_{60})_3^+$, (c) $M_3(C_{60})_4^+$, (d) $M_4(C_{60})_4^+$, and (e) $M_5(C_{60})_5^+$ (M = Sc, Ti, and V).

$V(CO)_6^+$ are 15 and 16, respectively, so the criterion of 16 VEs seems worthy to deduce an electronic structure by CO adsorption.

Assuming that C_{60} acts as a η^6-ligand, $Sc_1(C_{60})_1(CO)_4^+$ has 16 VEs, whereas $M_1(C_{60})_1(CO)_3^+$ has 15 (16) VEs for M = Ti(V). Here the superscripts of symbol η denote how many carbon atoms in C_{60} are bonded to a metal atom. If C_{60} behaves itself as a η^5-ligand, $Ti_1(C_{60})_1(CO)_3^+$ having 14 VEs should react with one more CO to satisfy the 16 VEs. Furthermore, since the metal−benzene complex of $M(C_6H_6)_1^+$ takes the same number of k_{max} toward CO as $M_1(C_{60})_1^+$, it is safely concluded that C_{60} acts as a η^6-ligand for Sc, Ti, and V.

On the other hand, $M_1(C_{60})_2^+$ has 14, 15, and 16 VEs for M = Sc, Ti, and V, respectively. According to the criterion of 16 VEs, $Sc_1(C_{60})_2^+$ can take one CO, but it shows no reactivity, as described above. This is probably because the steric hindrance of C_{60} avoids reacting with CO. In fact, $Sc(C_6H_6)_2^+$ is similarly nonreactive toward CO and O_2. In summary, in both $M(C_{60})_1^+$ and $M(C_{60})_2^+$ (M = Sc, Ti, and V), C_{60} bonds the metal atom at a hexagonal ring; $M(\eta^6\text{-}C_{60})_1^+$ and $M(\eta^6\text{-}C_{60})_2^+$. Furthermore, it is reasonable to extend this bonding scheme to that of the other dumbbell clusters; they can be expressed as $Sc_n(\eta^6\text{-}C_{60})_m^+$, $Ti_n(\eta^6\text{-}C_{60})_m^+$, and $V_n(\eta^6\text{-}C_{60})_m^+$. This conclusion on the binding site is rationalized again by measurement of ionization energy, as described below. As mentioned above, the similar magic number behavior was observed also in $C_n(C_{60})_m$ and the similar network structure was deduced, but the binding site seems different from that of M−C_{60}. Taking the diameter of a carbon atom into account, the C atom seems not to be located on the six-membered ring of C_{60}.

III.2.3. Structures of $M_n(C_{60})_m^+$ (M = Cr, Fe, Co, and Ni). Figure 9 shows typical examples of mass spectra of (a) $Cr_n(C_{60})_m^+$, (b) $Fe_n(C_{60})_m^+$, (c) $Co_n(C_{60})_m^+$, and (d) $Ni_n(C_{60})_m^+$ cluster cations produced by the foregoing procedure.[67,71] Mass peaks of the clusters are labeled according to the notation (n, m), denoting the number of metal atoms (n) and C_{60} (m). The main peaks in the spectrum are (n, m) = (0−1, 1), (1, 2), (1, 3), (2−4, 4), and (5, 5) for each m. The pattern in the mass spectrum differs from that of $V_n(C_{60})_m^+$, in which (n, n + 1) clusters (n = 1−3) are prominently abundant due to a chain structure between V atoms and C_{60}. To explain the mass spectrum of $M_n(C_{60})_m^+$, the adsorption reactivity of (1, 3) and (n, 4) was examined by the chemical probe method with various gases.

$M_1(C_{60})_3^+$ is abundant among species containing a single metal atom, while $(1, 3)^+$ is missing in the dumbbell clusters for M = Sc, Ti, and V.[68] In the chemical probe experiment,

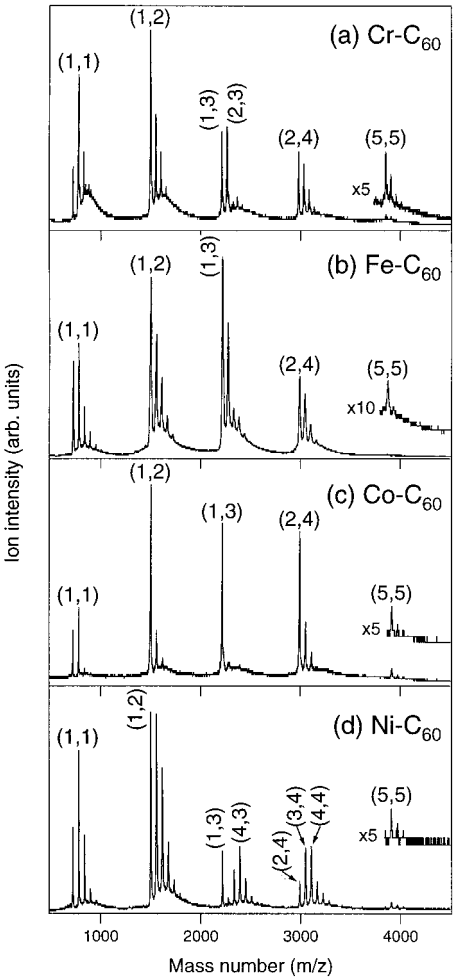

Figure 8. Time-of-flight mass spectra of (a) $Cr_n(C_{60})_m^+$, (b) $Fe_n(C_{60})_m^+$, (c) $Co_n(C_{60})_m^+$, and (d) $Ni_n(C_{60})_m^+$.

$M_1(C_{60})_3^+$ was nonreactive toward all of the gases, such as CO, O_2, C_2H_2, C_2H_4, C_6H_6, and NH_3, whereas quite minor peaks of $(n, 3)^+$ (n = 2) showed an occurrence of adsorption reaction into their adduct of $(n, 3)^+ + L$ (L = reactant gases). The adduct formation of $(n, 3)^+$ (n = 2) implies that the cluster possesses an exterior metal atom. Therefore, we proposed that $(1, 3)^+$ takes a tricapped planar structure, as shown in Figure 9a.

If $(1, 3)^+$ takes the tricapped planar structure, $(1, 2)^+$ should be bent to some extent as a precursor of (1, 3) because the Co atom of $(1, 2)^+$ in that configuration can afford to attach to the third C_{60}. When $(1, 1)^+$ and $(1, 2)^+$ were reacted with CO, they

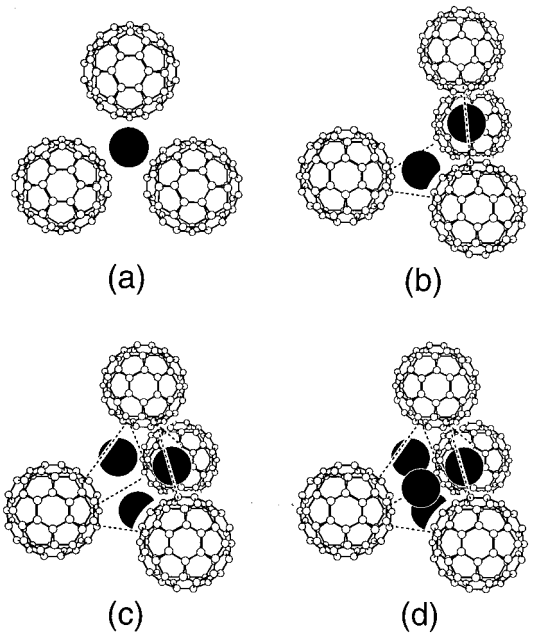

Figure 9. Proposed geometric structures: (a) $M_1(C_{60})_3^+$; (b) $M_2(C_{60})_4^+$; (c) $M_3(C_{60})_4^+$; (d) $M_4(C_{60})_4^+$. M (solid circle) denotes metal atoms Cr, Fe, Co, and Ni.

indeed resulted in CO adducts of $(1, 1)^+ + 3CO$ and $(1, 2)^+ + 2CO$, respectively. Figure 10 shows the adsorption reaction of Co^+, $Co(C_{60})_1^+$, and $Co(C_{60})_2^+$ toward CO, in which every set of two spectra is shown on the same intensity scale. Although the clusters were reacted with CO without mass-selection of the reaction precursor, the total ion intensity in every set seems almost conserved before/after the reactions within experimental uncertainties. Thus, it is reasonably assumed that the adsorption reaction mainly results in the CO adduct formation with negligible fragmentation. Comparison between $(1, 1)^+$ and $(1, 2)^+$ shows that the Co atom in $(1, 2)^+$ is not located on either C_{60}, because a Co atom on C_{60} can bond three CO molecules, as observed in $(1, 1)^+$. Then, the Co atom in $(1, 2)^+$ should bridge two C_{60}. The CO adduct formation shows the Co atom in $(1, 2)^+$ can bond another molecule, which is consistent with the $(1, 3)^+$ formation. As discussed in the preceding section, no reaction takes place for the linear dumbbell $V_1(\eta^6\text{-}C_{60})_2^+$ toward either CO.[66,68] Since the averaged dissociation energies of V^+-CO are similar to those of the Co^+ case, the adsorption reaction of $Co(C_{60})_2^+$ with CO should be attributed not to thermodynamical energetics, but to the bent structure. Therefore, it is concluded that the $(1, 2)^+$ cluster takes a bent structure, which results in the tricapped planar structure of $(1, 3)^+$ with the third C_{60}.

To get further information on the clusters having multimetal atoms, a similar chemical probe experiment was employed for the $(n, 4)^+$ series using reactant gases, CO and O_2. A typical example of the reaction toward O_2 is shown in Figure 11. The compositions of $(2, 4)^+$, $(3, 4)^+$, and $(4, 4)^+$ were nonreactive, although $(5, 4)^+$ and $(6, 4)^+$ were reactive. This result indicates that $(2, 4)^+$, $(3, 4)^+$, and $(4, 4)^+$ have no exterior Co atom in the clusters, because an exterior Co atom could react with O_2 as discussed above. We also obtained the same reactivity with CO. The inert reactivity does not directly offer conclusive evidence about the position of the cobalt atoms or whether the atoms are isolated by C_{60} or cluster with each other. Considering that the Co atom is favorably surrounded by three C_{60}, however, the plausible structures of $(2, 4)^+$, $(3, 4)^+$, and $(4, 4)^+$ can be presumed as shown in Figure 9b−d. The formation processes

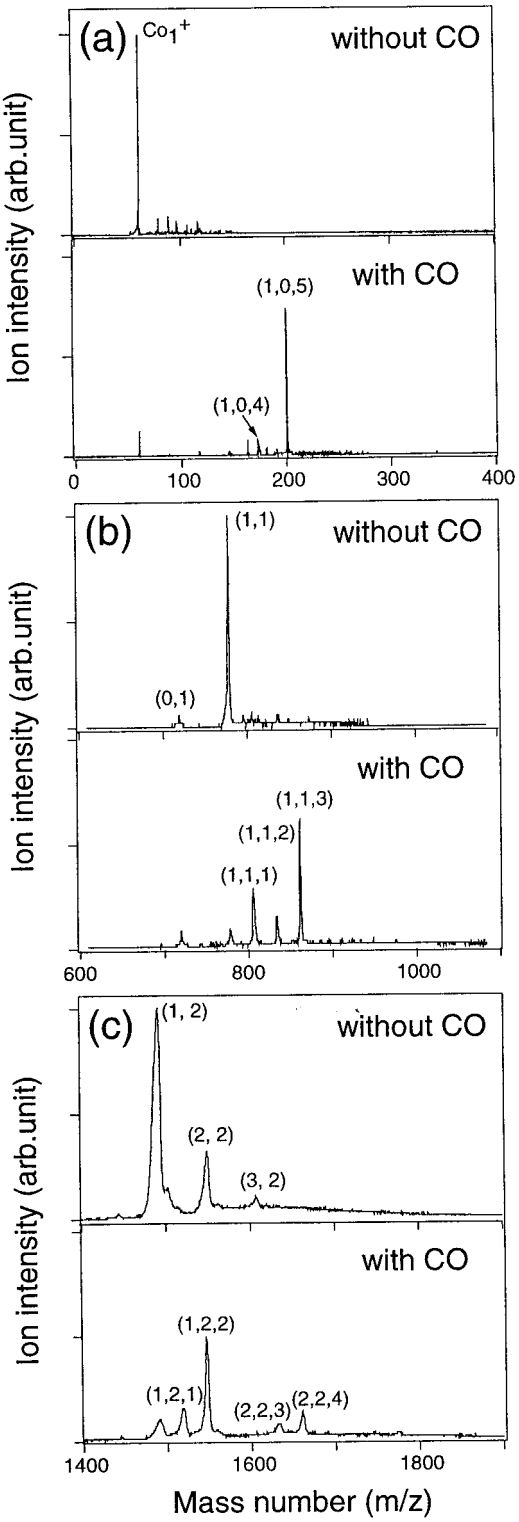

Figure 10. Time-of-flight mass spectra of $Co_n(C_{60})_m^+$ before and after adsorption reaction with CO: (a) Co_1^+; (b) $Co_1(C_{60})_1^+$; (c) $Co_1(C_{60})_2^+$. The most intense peak in each spectrum before the reaction is normalized. The product compositions are expressed by (n, m, k) for $Co_n(C_{60})_m(CO)_k^+$.

of each cluster could be as follows: for $(2, 4)^+$, the first Co atom surrounded by three C_{60} forms the stable $(1, 3)^+$, and then the second Co atom forms another local $(1, 3)^+$ using the fourth C_{60}, which results in a double tricapped plane of $(2, 4)^+$, as shown in Figure 9b. For $(3, 4)^+$ and $(4, 4)^+$, the third and the fourth Co atoms form additional local $(1, 3)^+$ groups, resulting in the trigonal pyramid shown in Figure 9c,d. In $(4, 4)^+$, two

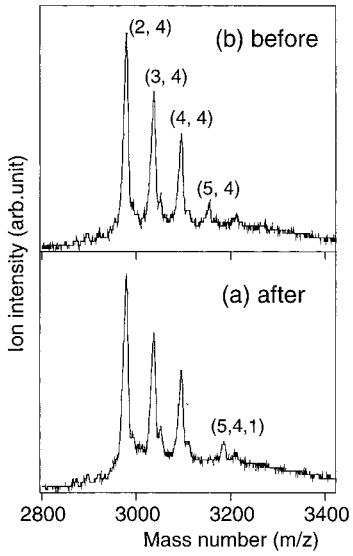

Figure 11. Time-of-flight mass spectra of $Co_n(C_{60})_4^+$, (a) after and (b) before oxidation reactions. The product compositions are expressed by (n, m, k) for $Co_n(C_{60})_m(O_2)_k^+$.

tetrahedra (trigonal pyramids) of Co_4 and $(C_{60})_4$ form a "face-centered tetrahedral structure" without bonds between Co atoms.

According to Hoffmann et al.,[90] the trigonal pyramid Co_4 cluster is calculated to be stable in bulk C_{60}, in which the four apexes of the Co_4 cluster point to the outer apexes of a local $(C_{60})_4$ trigonal pyramid in the bulk C_{60} lattice; the trigonal pyramid of Co_4 is inside the trigonal pyramid of $(C_{60})_4$. Then, our proposition for the (4, 4) cluster differs from theirs because the metal−metal bonding is not assumed and the apexes of four Co (not cluster) are located at the center of each $(C_{60})_3$ face. Although either geometry is conceivable, the plausible structure for (4, 4) seems to be our proposed pyramid structure, because the (3, 3) cluster never appears in our mass spectrum. If (4, 4) consists of a Co_4 cluster core at the center, as proposed by Hoffmann et al., (3, 3) having a Co_3 cluster core should also be observed in the mass spectrum. The missing of (3, 3) implies that the four Co atoms in (4, 4) are isolated by C_{60}. In the gas phase, it seems reasonable that the different structure for (4, 4) becomes stable due to the lack of packing factors in the lattice.

Thus, $(1, 3)^+$ takes a tricapped planar structure in which the Cr atom is surrounded by three C_{60} (Figure 9a). The stable $(1, 3)^+$ cluster is generally observed in the late transition metal−C_{60} complexes, such as Fe−C_{60}, Co−C_{60}, Ni−C_{60}, and Cu−C_{60}.[71] Namely, there is a distinction between V and Cr whether the metal atom is bicapped or tricapped by C_{60}. If C_{60} behaves itself only as the η^6-ligand, the Cr atom should result in the stable structure of bicapped dumbbell as similar to the bis-(benzene)chromium molecule, $Cr(C_6H_6)_2$, which satisfies the 18-electron rule. On the basis of the 18-electron rule, the formation of $Cr(C_{60})_3^+$ indicates that not all of the C_{60} in it acts as the η^6-ligand. According to theoretical estimation, performed with the approximate molecular orbital method partial retention of diatomic differential overlap (PRDDO),[91] C_{60} is an inferior η^6-ligand compared to benzene due to reduced metal−ligand overlap. This nature may result in forming stable $(1, 3)^+$ even for Cr. As pointed out later, C_{60} is able to act as a η^3-ligand in Co−C_{60}.[67] Then, the most probable structure is $Cr(\eta^6\text{-}C_{60})_1(\eta^3\text{-}C_{60})_2$ which satisfies the 18-electron rule; the three C_{60} are not equivalent. In fact, the ligand of η^6-C_{60} is suggested by low ionization energy of (1, 3), as described in section III.2.4.

When Cr−C_{60} and Co−C_{60} are compared, the mass distributions are different especially at $(2, 3)^+$. $(2, 3)^+$ for Cr−C_{60} has enough intensity to be detected, while $(2, 3)^+$ for Co−C_{60} is very weak and $(n, 3)^+$ are scarcely produced at $n = 2$.[67] This difference indicates that the chainlike structure might contribute to form stable $Cr_2(C_{60})_3^+$ (Figure 7b). For the C_{60} complex of early transition metals, a linear chain or a ring structure is preferable, whereas for late transition metals a three-dimensional lump structure becomes preferable. Cr is located at the border between early and late transition metals, so that Cr−C_{60} seemingly takes the chainlike structures as well as the lump structures.

As shown in Figure 10, every cluster of (1, 0), (1, 1), and (1, 2) of Co−C_{60} has a specific maximum number of CO molecules adsorbed (k_{max}). The specific numbers of k_{max} are 5, 3, and 2 for (1, 0), (1, 1), and (1, 2), respectively. On the basis of the 18 valence electrons (VEs) rule for organometallic compounds,[86] the number of VEs allotted to C_{60} can be counted. For (1, 0), five CO molecules completely satisfy the 18 VEs rule, and then the 18 VEs rule predicts that C_{60} donates 4 and 3 electrons in (1, 1) and (1, 2), respectively. Similarly, C_{60} donates 3(4) electrons in (1, 3) according to the 18 VEs rule. Although C_{60} consists of five- and six-membered rings, these results clearly show that C_{60} never acts as a η^5- or η^6-ligand in the Co−C_{60} clusters. The most likely number of VEs for C_{60} is 3 in the Co−C_{60} cluster; that is to say, C_{60} acts as a 3-electron-donor for the Co atom. Since in the dumbbell structure of $Sc_n(C_{60})_m^+$, $Ti_n(C_{60})_m^+$, and $V_n(C_{60})_m^+$ C_{60} acts as a 6-electron-donor,[66,68] the result of the Co−C_{60} clusters implies that the bonding nature of C_{60} depends on metal elements. In fact, Freiser and co-workers observed the formation of $FeC_{60}(CO)_4^+$, instead of $FeC_{60}(CO)_5^+$, as a product of the reaction between C_{60}^+ and $Fe(CO)_5$, which suggests that C_{60} can be either a η^2- or η^3-ligand.[92] These results may indicate that C_{60} molecules ligate either with the hexagonal rings donating only three electrons, or with the pentagonal rings, depending on the metal element involved. Interestingly, the partial ligation of C_{60} reasonably explains the distinct stability of (1, 1) + C_6H_6 electronically as $Co(\eta^3\text{-}C_{60})_1(\eta^6\text{-}C_6H_6)_1$ based on the 18-electron rule.

Very recently, Duncan and co-workers have reported the production of $Ag_n(C_{60})_m^+$ by laser vaporization of a C_{60}-film-coated Ag rod.[42] Their photodissociation experiments of $Ag_n(C_{60})_m^+$ showed that $Ag(C_{60})_2^+$ most likely has a sandwich structure and that $Ag_3(C_{60})^+$ is represented as a silver trimer cation bound electrostatistically to C_{60}. Although the observed $Ag(C_{60})_2^+$ may not take a linear structure in comparison with our results of $Cu_n(C_{60})_m^+$, the information on the binding site is indispensable to examine the geometry spectroscopically.

III.2.4. Ionization energies of $M_1(C_{60})_m$ and $M_1(C_{60})_m(Bz)_k$. The ionization energies (E_i's) of neutral $M_n(C_{60})_m$ clusters ($n = 1-3$ and $m = 1-4$; M = Sc, Ti, V, and Cr) were determined by a photoionization spectroscopic method, including those of their benzene complexes, which are tabulated in Table 1.[68] The E_i's of $Sc_1(C_{60})_1(Bz)_1$, $V_1(C_{60})_1(Bz)_1$, $Cr_1(C_{60})_2$, and $Cr_1(C_{60})_1(Bz)_1$ were determined from the final decline of the PIE curves, although the others were determined from their appearance photon energy, because it was difficult to obtain the PIE curve for them being close to the limit of the tunable range of the UV laser. The E_i's for all of the $M_1(C_{60})_1$ and larger clusters having $n = 2$ were higher than 5.92 eV, and lower than 6.42 eV.

All the E_i values of the tabulated clusters are lower than those of the metal atoms (Sc, 6.54 eV; Ti, 6.82 eV; V, 6.74 eV; Cr, 6.76 eV), C_{60} (7.61 eV), and C_6H_6 (9.24 eV).[77] Moreover, the E_i of the $M_1(C_6H_6)_2$ is similar to those of $M_1(C_{60})_1(Bz)_1$ and $M_1(C_{60})_2$. The similarity in E_i's of $M_1(C_{60})_x(Bz)_y$ $(x + y = 2)$

evidently shows that the metal atom is sandwiched between the six-membered rings of C_{60} rather than the five-membered rings. In fact, E_i becomes much higher in a bis(cyclopentadienyl) complex (for example, $V_1(C_5H_5)_2$; $E_i = 6.78$ eV), where the M atom is sandwiched between the five-membered rings. It generally can be seen that the interaction with η^6-C_{60} results in relatively low E_i of 5.5−5.7 eV. As shown in Figure 4a,[60,62] the E_i value of the $M_n(Bz)_{n+1}$ sandwich cluster decreases greatly with the number n; the E_i's of $V_n(Bz)_{n+1}$ 5.75, 4.70, 4.14, and 3.83 eV for $n = 1$, 2, 3, and 4. However, the E_i value of the $M_n(C_{60})_{n+1}$ dumbbell cluster for M = Sc and V never decreases with the cluster size. The reason is probably attributed to the difference in the interaction between d electrons of the metal atom and the π electron of the carbon ring; the d−π interaction is discontinuous in $M_n(C_{60})_m$, while it is continuous in $M_n(Bz)_m$ along a molecular axis.

As discussed above, the ionization energy (E_i) of the early transition metal (M_E)−C_{60} cluster is a good index to gain an understanding of the d−π interaction. In contrast to $(M_E)_n(C_{60})_m$, the $Fe_n(C_{60})_m$, $Co_n(C_{60})_m$, and $Ni_n(C_{60})_m$ clusters could not be ionized by the ArF excimer laser (6.42 eV). Without benzene, no photoions of $M_n(C_{60})_m^+$ for M = Fe, Co, and Ni were observed via one-photon ionization of the ArF laser, whereas photoionized product ions with benzene were observed, for example, at (n, m, k) = (2, 1, 2), (3, 1, 3), (2, 2, 1), and (3, 2, 2) for $Co_n(C_{60})_m(Bz)_k$. The low E_i of the benzene complex is characteristic of the d−π interaction, and the addition of benzene decreases the E_i's of $M_n(C_{60})_m$. Thus, the high E_i's of the late transition metal (M_L)−C_{60} clusters imply that the interaction of M_L−C_{60} is weaker than that of M_L−C_6H_6, especially in cationic states. For Sc−C_{60}, Ti−C_{60}, and V−C_{60},[66,68] in which C_{60} is a η^6-ligand for metal atoms, their E_i's are low, around 5.8 eV. Therefore, we conclude that C_{60} is not a η^6-ligand in M_L−C_{60}. For Cr−C_{60}, however, the E_i of the tricapped $Cr_1(C_{60})_3$ is exceptionally similar to those of the bicapped $M(C_{60})_2$ (M = Sc, Ti, V, and Cr). The E_i of $Cr_1(C_{60})_3$ presents a great contrast with those of other $M_1(C_{60})_3$ (M = Fe, Co, and Ni); all the E_i's of $Fe_1(C_{60})_3$, $Co_1(C_{60})_3$, and $Ni_1(C_{60})_3$ are above 6. 42 eV, in which C_{60} acts as η^3-ligand.[67,71] Then, the low E_i of $Cr_1(C_{60})_3$ (5.71 eV) is reasonably attributed to that one of C_{60} acts as the η^6-ligand in $Cr_1(C_{60})_3$, which is pointed out in the preceding section. This fact implies that the d−π interaction at the η^6-ligand should result in larger stabilization in a cationic state than that in a neutral state. These results on the E_i's of M−C_{60} can be explained by the binding site on C_{60}, which is consistent with those of the chemical probe experiments.

III.3. Lanthanide−COT Clusters. *III.3.1. Mass Spectra of $Ln_n(COT)_m$ Complexes.* Parts a−d of Figure 12 show typical examples of the photoionization mass spectra of $Ln_n(COT)_m$ [Ln = lanthanide metals of Nd, Eu, Ho, and Yb and COT = 1,3,5,7-cyclooctatetraene (C_8H_8); henceforth (n, m)] produced by the foregoing procedure. Main peaks in each spectrum showed almost the same compositions denoted as (n, $n + 1$). Even when the concentration of COT vapor was changed to higher one, these main peaks remained unchanged in the mass spectra. Therefore, these (n, $n + 1$) species are indeed abundant and stable complexes formed in the saturatedly high concentration of COT.

The most probable structure is a multiple-decker sandwich structure by analogy to the structure of the transition metal−benzene complexes,[60,76] in which lanthanide metal atoms and COT molecules are alternately pile up. In fact, it is natural to extend the single sandwich structure into multiple sandwich one, because the triple-decker structure of Ce−COT or Nd−COT

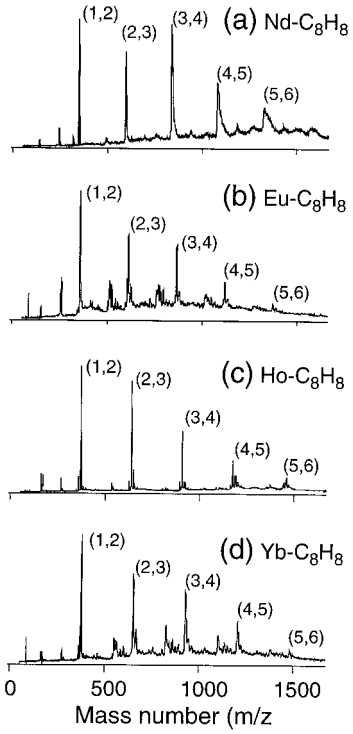

Figure 12. Time-of-flight mass spectra of lanthanide (Ln)−1,3,5,7-cyclooctatetraene (C_8H_8; COT) complexes, $Ln_n(C_8H_8)_m$ [Ln = (a) Nd, (b) Eu, (c) Ho, and (d) Yb] obtained by the photoionization of the ArF laser (6.42 eV). Peaks are labeled according to the notations (n, m), denoting the number of Ln atoms (n) and COT molecules (m).

was actually prepared in the condensed phase.[93,94] Since the advantage of the gas phase synthesis is no environmental factors such as organic solvents, it seems that these novel structures of Ln−COT can possibly come true as well as those of M−Bz and M−C_{60}.

III.3.2. Photoelectron Spectroscopy of $Ln(COT)_2^-$ Anions. To elucidate further bonding nature of these complexes, we measured photoelectron spectra of the anions, $Ln(C_8H_8)_2^-$, at 266 nm (4.66 eV) for Ln = Ce, Nd, Eu, and Yb (Figure 13). In the PES spectra, the horizontal axis corresponds to an electron binding energy, E_b, which is defined as $E_b = h\nu - E_k$, where E_k is a kinetic energy of the photoelectron and $h\nu$ is a photon energy of the photodetachment laser. A downward arrow indicates photodetachment threshold energy, E_T, value in each figure, and the E_T value corresponds to upper limits of the adiabatic electron affinity, E_A. Besides the E_T values, vertical detachment energies (VDEs) of the peaks are also derived from the peak maxima in the photoelectron spectra. E_T's and VDEs are tabulated in Table 3, including VDEs of successive peak-(s). The successive peaks correspond to the photodetachment into the electronically excited states of the corresponding neutral.

At the first glance of the four photoelectron spectra, striking similarity is readily found and they are classified into two groups; one is $Ce(COT)_2$ and $Nd(COT)_2$ and the other is $Eu(COT)_2$ and $Yb(COT)_2$. In the former group, two peaks are located around the binding energy of 2.5 and 3.5 eV, and they have similar profiles with a sharp leading edge and a couple of shoulder on the higher binding energy side. In the latter one, the first two sharp peaks are located around 2.0 and 2.5 eV. The similarity in these two groups is ascribed to a common electronic feature; they are characterized as a highly ionic complex that depends not on the metal elements, but on the number of oxidation state. It is reasonable to assume that all of Ce and Nd take the oxidation state of +3, while both Eu and

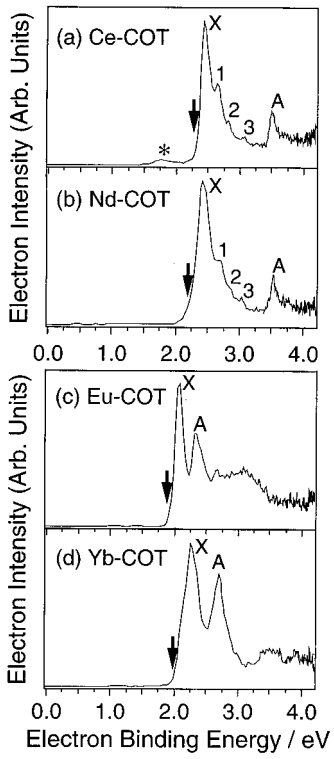

Figure 13. Photoelectron spectra of $Ln(COT)_2^-$ (Ln = (a) Ce, (b) Nd, (c) Eu, and (d) Yb) at 266 nm (4.66 eV). Arrows indicate threshold energies (E_T). Bands X and A correspond to the transition into the electronic ground state and first electronic excited state, respectively.

TABLE 3: Threshold Energy (E_T) and the Vertical Detachment Energy (VDE) of $Ln(COT)_2^-$ Complexes (eV)[a]

Ln	E_T		VDE
Ce	2.42(32)	X	2.50
		A	3.55
Nd	2.37(25)	X	2.47
		A	3.54
Eu	2.02(09)	X	2.14
		A	2.68
Yb	1.95(10)	X	2.13
		A	2.65

[a] Numbers in parentheses indicate experimental uncertainties; 2.42(32) represents 2.42 ± 0.32.

Yb take that of +2, by analogy to the reported lanthanide complexes.[48,53−56,93−95]

As well-known by $4n + 2$ rule of aromatics, a COT molecule can act as an electron acceptor by two electrons.[26] In fact, all of $Ce(COT)_2$ and $Nd(COT)_2$ in bulk materials have been prepared as alkali metal salts denoted as $M_{alkali}^+[Ln^{3+}(COT^{2-})_2]$,[48,53] and then it is rational to consider that the anions of $[Ln(COT)_2^-]$ can be expressed as a $Ln^{3+}(COT^{2-})_2$ configuration for Ce and Nd. Since each COT molecule has two excess electrons, the $(1, 2)^-$ should become stable with the electronic demands of Ln^{3+} and COT^{2-}.

In the oxidation states of 3+, Ce^{3+} and Nd^{3+} have 1 and 3 f electron(s), respectively, but this difference does not change the spectra, as shown in their photoelectron spectra. This is because the bands in the spectra come predominantly from the molecular orbital of the ligand molecules. By analogy to the photoelectron spectra of cerocene obtained by He I, the bands of X and A are undoubtedly associated with electron detachment from the e_{2u} and e_{2g} molecular orbitals, respectively.[96,97] The fine structures associated with the band X is probably due to vibrations of the COT ligands in the neutral lanthanocene.

For Ln = Ce and Nd, the anions of $Ln(COT)_2^-$ are reasonably assumed to have D_{8h} symmetry in the gas phase, because the COT^{2-} ligands satisfy the planar aromaticity with Ln^{3+}.[98] Indeed, the symmetry of D_{8h} has been found by crystal studies for alkali metal salts of $M_{alkali}[Ln(COT)_2]$.[1−4] Under the representations of the D_{8h} point group, the most important covalent contributions to metal−ring bonding may arise from metal 5d(e_{2g}) and 4f(e_{2u}) orbitals interacting with the high-lying π orbitals (e_{2u}, e_{2g}) of the COT ligands. For cerocene$^+$ produced by the photoionization of cerocene, it was reported that the energy gap between e_{2u} and e_{2g} MOs is 0.93 eV.[96] As listed in Table 3, on the other hand, the gaps are 1.05 and 1.07 eV for the neutral $Ce(COT)_2$ and $Nd(COT)_2$,. The larger gap of the neutral cerocene compared to that of cerocene$^+$ should be attributed to the stronger ionic interaction; Ce^{3+} interacts with two $COT^{1.5-}$ in the neutral, whereas Ce^{3+} does with two $C_8H_8^-$ in the cation.

As shown in Figure 13, the photoelectron spectra of $Eu(COT)_2^-$ and $Yb(COT)_2^-$ are very similar each other, although they are different from those of $Ce(COT)_2^-$ and $Nd(COT)_2^-$. This difference is reasonably attributed to the difference in the oxidation states. Eu and Yb are typical examples for stable Ln^{2+} complexes in bulk materials. Their $Ln(COT)_2$ compounds are prepared as salts having two alkali atoms such as $(M_{alkali}^+)_2[Ln^{2+}(COT^{2-})_2]$. This is because Eu and Yb possess $4f^7$ and $4f^{14}$ configurations in the oxidation states of 2+, which corresponds to the half-filled and filled 4f orbitals stabilized by the spin−spin exchange interaction, respectively. Therefore, their neutrals are considered to take $Eu^{2+}(COT^-)_2$ and $Yb^{2+}(COT^-)_2$ configurations. Change of electronic and vibrational structures is ascribed to the change of electronic configuration of COT from $(COT^{1.5-})_2$ to $(COT^-)_2$. In the photoelectron spectra, two strong bands were observed and their gaps are 0.54 eV for neutral $Eu(COT)_2$ and 0.52 eV for neutral $Yb(COT)_2$. On the basis of the assignment for $Ce(COT)_2^-$ and $Nd(COT)_2^-$, the two bands in $Eu(COT)_2^-$ and $Yb(COT)_2^-$ are assigned to those from e_{2u} and e_{2g}, respectively, although it seems that the neutral $Eu(COT)_2$ and $Yb(COT)_2$ have lower symmetry than D_{8h} due to deformation of the eight-membered ring of COT.

Since the stability of Eu^{2+} is ascribed to the half-filled 4f orbitals, $Eu(C_8H_8)_2$ should evidently have the high multiplicity of electron spin. Although it is difficult to define the symmetry of the ground state at the present stage, the high electron spin should result in a high value of the total angular momentum, J, which directly offers a magnetic moment of the complex through the large spin−orbit coupling. The magnetic properties of Eu−COT including other Ln−COT complexes will also give invaluable information on the physics of the organolanthanide for the future.

III.3.3. Ionization Energy of the Neutral $Ln_n(C_8H_8)_{n+1}$ Complexes. For neutral and cationic Ln−COT complexes, larger complexes having $(n, n + 1)$ compositions were successfully produced as shown in Figure 12. To know the electronic properties, the ionization energies (E_i's) of the neutral $Ln_n(COT)_m$ were measured by using photoionization spectroscopy. From the final decline of the PIE curves, the E_i's of the other $Ln_n(COT)_{n+1}$ were measured and tabulated in Table 4.[69] For Eu and Yb complexes, they cannot be photoionized by 5.92 eV photons, but can be by 6.42 eV photons of the ArF laser.

When the size dependence of E_i is shown as in Figure 14, two patterns are easily distinguishable. For $Nd_n(COT)_{n+1}$ and $Ho_n(COT)_{n+1}$ (Figure 14a), the E_i's of (1, 2) and (2, 3) show similar values, but that of (3, 4) largely decreases by 0.8 eV.

TABLE 4: Ionization Energy (E_i) of Sandwich Complexes of $Ln_n(COT)_{n+1}$ ($n = 1-3$) in eV

Ln element	n	E_i [a]
Nd	1	5.06(2)
	2	5.02(3)
	3	4.15(5)
Eu	1, 2, 3	$5.92 < E_i < 6.42$
Ho	1, 2	$5.92 < E_i < 6.42$
	3	5.35(8)
Yb	1, 2	$5.92 < E_i < 6.42$
	3	$5.89 < E_i < 6.42$

[a] Numbers in parentheses indicate experimental uncertainties; 5.27(5) represents 5.27 ± 0.05. "$5.92 < E_i < 6.42$" means that lower and upper limits are 5.92 and 6.42 eV, respectively.

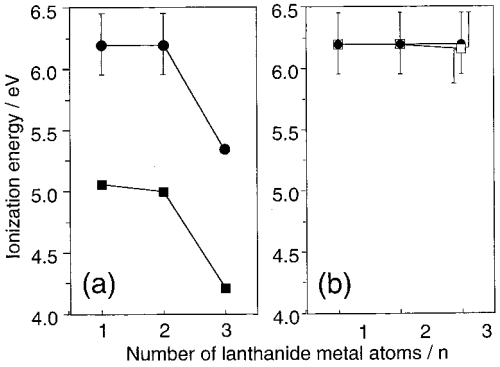

Figure 14. Ionization energies (E_i's) of multiple-decker sandwich complexes: (a) $Nd_n(COT)_{n+1}$ (solid square) and $Ho_n(COT)_{n+1}$ (solid circle); (b) $Eu_n(COT)_{n+1}$ (solid circle) and $Yb_n(COT)_{n+1}$ (open square).

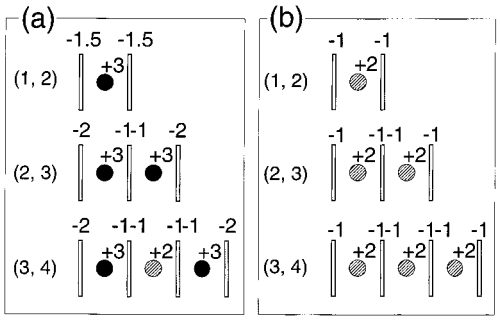

Figure 15. Allotment of valence electrons of $Ln_n(C_8H_8)_{n+1}$ complexes: (a) Ln = Nd and Ho; (b) Ln = Eu and Yb. These schematics are based on the assumption of the 2 electron acceptability of C_8H_8 and multiply charged positive Ln ions (Ln^{3+} for Nd and Ho, and Ln^{2+} for Eu and Yb).

For $Eu_n(COT)_{n+1}$ and $Yb_n(COT)_{n+1}$ (Figure 14b), however, the E_i values keep almost constant for $n = 1-3$, although the values have relatively large uncertainty. The two different size dependences can be explained by the charge distribution, based on the multiple ionic states in the complex. Considering that Ln atoms favor the Ln^{3+} or Ln^{2+} state in the ligand field, the distribution of valence electrons in multiple-decker $Ln_n(COT)_{n+1}$ results in those shown in Figure 15. In the case of Nd and Ho, Ln atoms can exist as Ln^{3+} ions interposed by COTs for $n = 1$ and 2. In $n = 3$, however, one of the Ln atoms in the multiple-decker structure cannot become the Ln^{3+} ion because of the lack of electron acceptability in the COT ligands. Then the central Ln atom should become a Ln^{2+} ion. When we look at the tendency of E_i's, E_i drops at $Ln_3(C_8H_8)_4$ (Ln = Nd and Ho) can be reasonably explained by the change of valence electrons as follows: Since the center Ln atom in (3, 4) should take the Ln^{2+} ion in neutral, large stabilization is expected for the cationic $(3, 4)^+$, by changing the charge from Ln^{2+} to Ln^{3+}. For Eu and Yb, on the other hand, complexes can by keeping the Ln^{2+} ion, as shown in Figure 15b. In a larger sandwich complex ($n = 3$), therefore, the oxidation state always becomes 2+ for the Ln atoms around the core of the neutral complex, while terminal Ln atoms in both ends are 3+. It is well-known that some of the Ln atoms, notably Tb, Ho, and Eu, show characteristic strong emission bands from the visible to ultraviolet region, and the energies and intensities depend on the oxidation states of 2+ and 3+. Then, the mixing of the different oxidation states in the complex seemingly leads to the combinations of the optical properties.

As shown in Figure 4a, the multiple-decker sandwiches of $M_n(Bz)_{n+1}$ (M = Sc, Ti, and V; $n = 1-4$),[60,62] E_i's showed a drastic decrease as the complex size increased. In $Ln_n(COT)_{n+1}$, however, an orbital contributing to the ionization process is considered to be discontinuous along the molecular axis, because the complex is bonded through ionic bonds and the charge is localized at each component. Since the first ionization is expected to occur from 4f(Ln) orbitals in (1, 2),[96] we concluded that the 4f orbital in the complex is localized and scarcely interacts with neighboring Ln atoms in the complex. According to the theoretical calculation of Dolg and co-workers,[56] $Nd(COT)_2$ is a charge-transfer complex in which three of six electrons in $Nd(6s^24f^4)$ transfer almost completely to 2COT, resulting in a configuration of $Nd^{3+}(COT^{1.5-})_2$. In the case of Eu and Yb, rather high E_i's of $Eu_n(COT)_{n+1}$ and $Yb_n(COT)_{n+1}$ seem to ensure complete charge transfer, although we are unaware of the extent of the charge transfer in the complexes. We conclude from all the results that bondings in $Ln_n(COT)_{n+1}$ are ionic in character, in which Ln atoms exist as Ln^{3+} or Ln^{2+} ions. Moreover, the multiply ionic character for the $Ln-C_8H_8$ complexes strongly suggests that the binding energy between the Ln atoms and the ligand molecules are much stronger that of the $V-C_6H_6$ complex, which was estimated to be 1−2 eV.

III.4. Lanthanide-C_{60} Clusters. *III.4.1. Mass Spectra of $Ln_n(C_{60})_m$ Complexes.* Figure 16 shows mass spectra of (a) $Eu_n(C_{60})_m^+$ and (b) $Ho_n(C_{60})_m^+$ cluster cations produced by the ablation of Ln (Ln = Eu or Ho) and C_{60} targets.[99] Peaks of the cationic clusters are labeled according to the notation $(n, m)^+$, denoting the number of Ln atoms (n) and C_{60} (m). Under this condition, the contribution of the Ln_n^+ cluster to $Ln_n(C_{60})_m^+$ formation was negligible because the abundance of the Ln_n^+ clusters ($n = 2$) was less than 1/1000 compared with that of the Ln^+ atoms. Both mass spectra indicate a common pattern of prominent peaks. The prominent peaks in the mass spectra correspond to $(n, m) = (1, 4)^+$, $(2, 5)^+$, $(3, 6)^+$, and $(4, 7)^+$, which are expressed as $(n, n + 3)^+$ ($n = 1-4$). The stability of $(n, n + 3)^+$ species are generally observed in the lanthanide−C_{60} clusters such as Ce−C_{60}, Nd−C_{60}, and Yb−C_{60}.[99] The mass distribution of these clusters remained unchanged even when the concentration of Ln atoms was increased with a higher laser fluence for the Ln rod. Moreover, we observed a similar pattern in the mass spectra of anionic and neutral as well as cationic Ln−C_{60} clusters. This fact implies that all of the cationic, anionic, and neutral Ln−C_{60} clusters composed of $(n, n + 3)$ ($n = 1-4$) have common structures. The magic numbers for Ln−C_{60} cluster cations are different from those of the other organometallic clusters such as M_T-C_{60}, $M_T-C_6H_6$, and Ln−COT.

In the chemical probe experiments, the clusters of $Ln_n(C_{60})_{n+3}^+$ were nonreactive toward both O_2 and CCl_4. No reactivity of $(n, n + 3)^+$ implies that they should have no exterior Ho atoms. Then, the Ho atom in $(n, n + 3)^+$ could be geometrically blocked by the surrounding C_{60}s, and it is

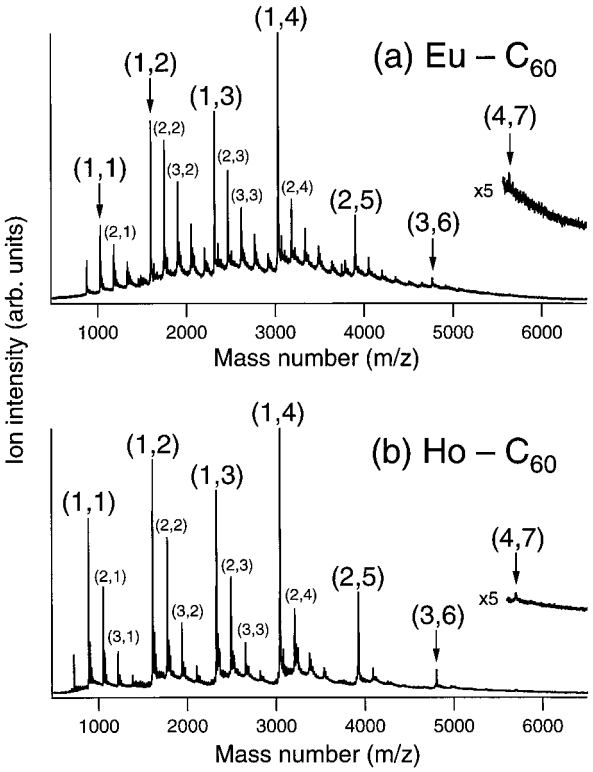

Figure 16. Time-of-flight mass spectra of (a) Eu−C_{60} and (b) Ho−C_{60} cluster cations. Peaks of the cluster cations are labeled according to the notation (*n*, *m*), denoting the number of metal atoms (*n*) and C_{60} molecules (*m*).

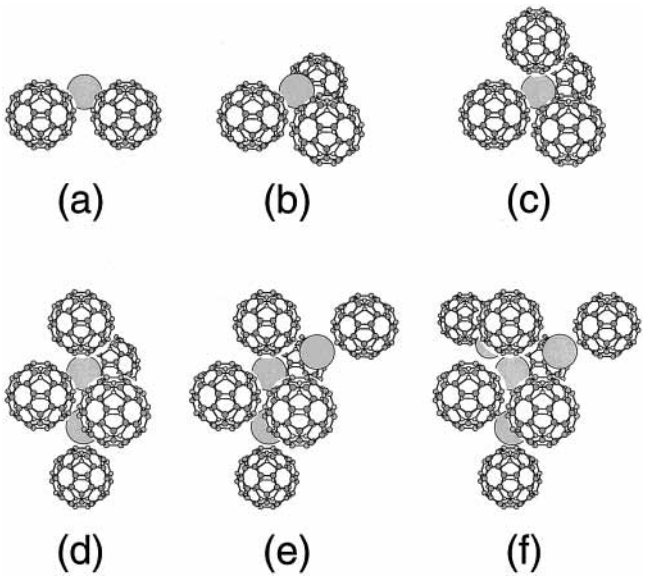

Figure 17. Proposed geometric structures: (a) $Ln_1(C_{60})_2$; (b) $Ln_1(C_{60})_3$; (c) $Ln_1(C_{60})_4$; (d) $Ln_2(C_{60})_5$; (e) $Ln_3(C_{60})_6$; (f) $Ln_4(C_{60})_7$ (Ln = Eu and Ho).

proposed that $(1, 4)^+$ forms a tetrahedral methane-like structure, as shown Figure 17. Since it is reasonably presumed that $(1, 4)^+$ is the smallest unit of $(n, n + 3)^+$ species, the plausible structures of the other $(n, n + 3)^+$ can be shown in Figure 17.

III.4.2. Photoelectron Spectroscopy of Ln(COT)$_2^-$ Anions. As mentioned above, the lanthanide complexes are well-known as charge transfer complexes where the Ln atoms are multiply charged cations and the ligands are charged anions. To deduce the electronic structure of Ln−C_{60} clusters, photoelectron spectroscopy of $Ln_1(C_{60})_m^-$ anions were performed. Figure 18

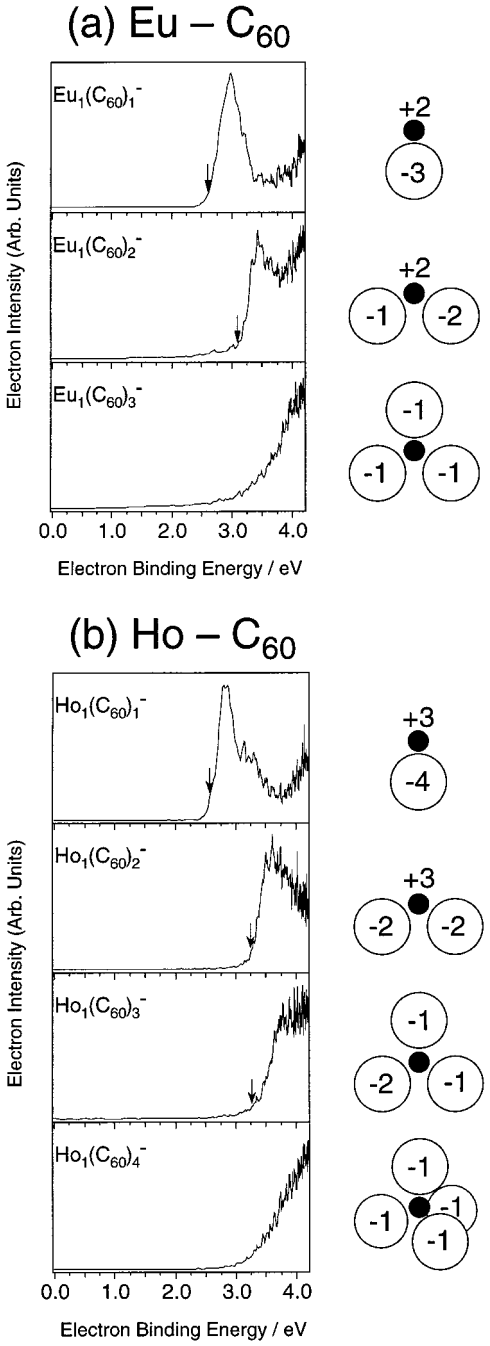

Figure 18. Photoelectron spectra of (a) $Eu_1(C_{60})_m^-$ ($m = 1-3$) and (b) $Ho_1(C_{60})_m^-$ ($m = 1-4$) measured at a photon energy of 4.66 eV (266 nm). The downward arrows indicate threshold energies, corresponding to electron affinities. Besides the spectra, allotment of valence electrons of $Ln_1(C_{60})_m^-$ are also shown schematically. These are based on the assumptions that the extra electron in $Ln_1(C_{60})_m^-$ anions localizes on C_{60} and that Eu and Ho atoms take the oxidation states of 2+ and 3+, respectively.

shows the photoelectron spectra of (a) $Eu_1(C_{60})_m^-$ ($m = 1-3$) and (b) $Ho_1(C_{60})_m^-$ ($m = 1-4$) at 266 nm (4.66 eV). The obtained EAs of $Eu_1(C_{60})_m$ and $Ho_1(C_{60})_m$ species are tabulated in Table 5. For $Eu_1(C_{60})_3$ and $Ho_1(C_{60})_4$, no effective photodetachment occurs at 266 nm due to the lack of the photon energy and only their lower limits of EAs are obtained to be 4.0 eV.

When the spectra of $Ln_1(C_{60})_m^-$ were compared as a function of the number of C_{60} molecules (*m*), it can be found that the EA of $Ho_1(C_{60})_3$ is almost the same as that of $Ho_1(C_{60})_2$, whereas the EA of $Eu_1(C_{60})_3$ is higher than that of $Eu_1(C_{60})_2$. This

TABLE 5: Electron Affinities of $Ln_1(C_{60})_m$ Clusters (Ln = Eu and Ho) in eV

cluster	Ln = Eu	Ln = Ho
$Ln_1(C_{60})_1$	2.61(12)[a]	2.56(12)
$Ln_1(C_{60})_2$	3.10(25)	2.24(19)
$Ln_1(C_{60})_3$	>4.0	3.25(21)
$Ln_1(C_{60})_4$		>4.0

[a] 2.61(12) represents 2.61 ± 0.12.

difference between Eu−C_{60} and Ho−C_{60} can be explained by the preferable oxidation states of these Ln atoms. Assuming that Eu and Ho atoms become Eu^{2+} and Ho^{3+}, respectively, the allotment of valence electrons in $Ln_1(C_{60})_m^-$ anions should be given in Figure 18. Here, it is reasonable to assume that the extra electron in the $Ln_1(C_{60})_m^-$ anions should be localized on C_{60}. Apparently, in the allotment, the EA of (1, 2) and (1, 3) for trivalent Ln should be the same, because they have the same charged C_{60}^{2-}. For Eu−C_{60} (Figure 5a), on the other hand, the monotonic increase in EA can similarly be rationalized by the charge distribution with Eu^{2+}, because the detached electron is released from different charged C_{60}; C_{60}^{3-} for $(1, 1)^-$, C_{60}^{2-} for $(1, 2)^-$, and C_{60}^- for $(1,3)^-$. This explanation successfully leads us to the conclusion that Eu and Ho atoms in $Ln_1(C_{60})_m$ clusters take 2+ and 3+ oxidation states, respectively. Then, it is concluded that the Ln−C_{60} clusters are formed through ionic bonding, distributing the valence electrons into the ligand molecules of C_{60}.

IV. Conclusions

In the gas phase, various network structures of organometallic clusters of M−Bz/C_{60} and Ln−COT/C_{60} were produced by the laser vaporization method. From the pattern of the predominant mass peaks and the chemical reactivity toward the gas reactant their sandwich or dumbbell structure was revealed, where metal atoms are separated and connected with the organic ligands. The electronic structures were studied and discussed by photoionization or photoelectron spectroscopy. Although both M_E−Bz and Ln−COT take on a similar multiple sandwich structure, the E_i of M_E−Bz is significantly lowered with the number of layers, while that of Ln−COT depends not on the number of layers but on the charge distribution. This difference is ascribed to the bonding nature; M_E−Bz is formed through a covalent bond and d electrons are delocalized along the molecular axis, whereas Ln−COT is formed through an fairly ionic bond, and the electronic state is expressed by the stacking of a local sandwich unit. As well as benzene, C_{60} can also act as an organic ligand and M−C_{60} forms a two- or three-dimensional novel network structure. The bonding in M_E−C_{60} arises from the interaction between d electrons of the metal atom and π electrons of the hexagonal carbon ring (η^6), giving superstructures of $V_n(\eta^6\text{-}C_{60})_m$. The regular arrangement of metal atoms in organometallic clusters should introduce useful properties, because the properties of bare metal atoms are modified by deliberately adding organic ligands. The gas-phase organometallic chemistry and physics can open up new aspects of chemical reaction, catalytic activity, and electron spin chemistry, and this area is one of the most promising for cluster materials.

Acknowledgment. The authors are grateful to Prof. S. Yabushita, Dr. K. Hoshino, Dr. T. Kurikawa, and Messers M. Hirano, T. Yasuike, K. Judai, Y. Negishi, S. Nagao, and K. Miyajima for their great contributions. This work is supported by a program entitled "Research for the Future (RFTF)" of Japan Society for the Promotion of Science (98P01203) and by a Grant-in-Aid for Scientific Research on Priority Areas from the Ministry of Education, Science, Sports, and Culture. A.N. sincerely expresses his gratitude to the Morino Foundation for partial financial support.

References and Notes

(1) Neuse, E. W.; Rosenberg, H. *Metallocene Polymers*; Marcel Dekker: New York, 1970; Chapter 3.
(2) Manners, I. *Adv. Organomet. Chem.* **1995**, *37*, 131.
(3) Teh, C. S.; Willey, K. F.; Robbins, D. L.; Pilgrim, J. S.; Duncan, M. A. *Chem. Phys. Lett.* **1992**, *196*, 233.
(4) Higashide, H.; Kaya, T.; Kobayashi, M.; Shinohara, H.; Sato, H. *Chem. Phys. Lett.* **1990**, *171*, 297.
(5) Holland, P. M.; Castleman, A. W., Jr. *J. Chem. Phys.* **1982**, *76*, 4195.
(6) Robels, E. S. J.; Ellis, A. M.; Miller, T. A. *J. Chem. Phys.* **1992**, *96*, 8791.
(7) Misaizu, F.; Sanekata, M.; Fuke, K.; Iwata, S. *J. Chem. Phys.* **1994,** *100*, 1161.
(8) Mitchell, S. A.; Blits, M. A.; Siegbahn, P. E. M.; Svensson, M. *J. Chem. Phys.* **1994**, *100*, 423.
(9) Kroto, H. W.; Heath, J. R.; O'Brien, S. C.; Curl, R. F.; Smalley, R. E. *Nature* **1985**, *318*, 162.
(10) Guo, B. C.; Wei, S.; Purnell, J.; Buzza, S.; Castleman, A. W., Jr. *Science* **1992**, *256*, 515.
(11) Guo, B. C.; Kerns, K. P.; Castleman, A. W., Jr. *Science* **1992**, *255*, 1411.
(12) Ervin, K. M.; Armentrout, P. B. *J. Chem. Phys.* **1985**, *83*, 166.
(13) Chen, Y.-M.; Armentrout, P. B. *Chem. Phys. Lett.* **1993**, *210*, 213.
(14) Meyer, F.; Khan, F. A.; Armentrout, P. B. *J. Am. Chem. Soc.*, **1995**, *117*, 9740.
(15) Jacobson, D. B.; Freiser, B. S. *J. Am. Chem. Soc.* **1984**, *106*, 3900.
(16) Hettich, R. L.; Jackson, T. C.; Stanko, E. M.; Freiser, B. S. *J. Am. Chem. Soc.* **1986**, *108*, 5086.
(17) Hettich, R. L.; Freiser, B. S. *J. Am. Chem. Soc.* **1987**, *109*, 3537.
(18) Afzaal, S.; Freiser, B. S. *Chem Phys. Lett.*, **1994**, *218*, 254.
(19) Willy, K. F.; Cheng, P. Y.; Bishop, M. B.; Duncan, M. A. *J. Am. Chem. Soc.* **1991**, *113*, 4721.
(20) Willy, K. F.; Yeh, C. S.; Robbins, D. L.; Duncan, M. A. *J. Am. Chem. Soc.* **1992**, *96*, 9106.
(21) Yeh, C. S.; Willy, K. F.; Robbins, D. L.; Duncan, M. A. *Int. J. Mass Spectrom. Ion Processes* **1994**, *131*, 307.
(22) Bauschlicher, C. W., Jr.; Partridge, H.; Langhoff, S. R. *J. Phys. Chem.* **1992**, *96*, 3273.
(23) Fagan, P. J.; Calabrese, J. C.; Malone, B. *Science* **1991**, *252*, 1160.
(24) Hawkins, J. M. *Acc. Chem. Res.* **1992**, *25*, 150.
(25) Balch, A. L.; Catalano, V. J.; Lee, J. W. *Inorg. Chem.* **1991**, *30*, 3980.
(26) Douthwaite, R. E.; Green, M. L. H.; Stephens, A. H. H.; Turner, J. F. C. *J. Chem. Soc., Chem. Commun.* **1993**, 1522.
(27) Chai, Y.; Guo, T.; Jin, C.; Haufler, R. E.; Chibanante, L. P.; Fure, J.; L. Wang, L.; Alford, J. M.; Smalley, R. E. *J. Phys. Chem.* **1991**, *95*, 7564.
(28) Caldwell, K. A.; Giblin, D. E.; Hsu, C. S.; Cox. D.; Gross, M. L. *J. Am. Chem. Soc.* **1991**, *113*, 8519.
(29) McElvany, S. W. *J. Phys. Chem.* **1993**, *96*, 4935.
(30) Haddon, R. C. *Nature* **1991**, *350*, 320.
(31) Hebard, A. F.; Rosseinsky, M. J.; Haddon, R. C.; Murphy, D. W.; Glarum, S. H.; Palstra, T. T. M.; Ramirez, A. P.; Kortan, A. R. *Nature* **1991**, *350*, 600.
(32) Holczer, K.; Klein, O.; Huang, S.-M.; Kaner, R. B.; Fu, K.-J.; Whetten, R. L.; Diederich, F. *Science* **1991**, *252*, 1154.
(33) Benning, P. J.; Martins, J. L.; Weaver, J. H.; Chibante, L. P. F.; Smalley, R. E. *Science* **1991**, *252*, 1417.
(34) Benning, P. J.; Poirier, D. M.; Ohno, T. R.; Chen, Y.; Jost, M. B.; Stepniak, F.; Kroll, G. H.; Weaver, J. H.; Fure, J.; Smalley, R. E. *Phys. Rev. B* **1992**, *45*, 6899.
(35) Hawkins, J. M.; Meyer, A.; Lewis, T. A.; Loren, S.; Hollander, F. J. *Science* **1991**, *252*, 312.
(36) Roth, L. M.; Huang, Y.; Schwedler, J. T.; Cassady, C. J.; Ben-Amotz, D.; Kahr, B.; Freiser, B. S. *J. Am. Chem. Soc.* **1991**, *113*, 6298.
(37) Roth, L. M.; Huang, Y.; Schwedler, J. T.; Cassady, C. J.; Ben-Amotz, D.; Kahr, B.; Freiser, B. S. *J. Am. Chem. Soc.* **1991**, *113*, 6298.
(38) Huang, Y.; Freiser, B. S. *J. Am. Chem. Soc.* **1991**, *113*, 8186.
(39) Huang, Y.; Freiser, B. S. *J. Am. Chem. Soc.* **1991**, *113*, 9418.
(40) Jiao, Q.; Huang, Y.; Lee, S. A.; Gord, J. R.; Freiser, B. S. *J. Am. Chem. Soc.* **1992**, *114*, 2726.
(41) Zimmerman, P. A.; Hercules, D. M. *Appl. Spectrosc.* **1993**, *47*, 1545.

(42) Reddic, J. E.; Robinson, J. C.; Duncan, M. A. *Chem. Phys. Lett.* **1997**, *279*, 203. (b) Buchanan, J. W.; Grieves, G. A.; Reddic, J. E.; Duncan, M. A. *Int. J. Mass Spectrom.* **1999**, *182/183*, 323.
(43) Zimmermann, U.; Malinowski, N.; Burkhardt, A.; Martin, T. P. *Carbon*, **1995**, *33*, 995.
(44) Tast, F.; Malinowski, N.; Frank, S.; Heinebrodt, M.; Billas, I. M. L.; Martin, T. P. *Phys. Rev. Lett.* **1996**, *77*, 3529.
(45) Basir, Y.; Anderson, S. L. *Electrochem. Soc. Proc.* **1995**, *95*−*10*, 1448.
(46) Marks, T. J. *Prog. Inorg. Chem.* **1978**, *24*, 51.
(47) Green, J. C. *Struct. Bonding* **1981**, *43*, 64.
(48) Schumann, H.; Meese-Marktscheffel, J. A.; Esser, L. *Chem. Rev.* **1995**, *95*, 865.
(49) Marks, T. J.; Ernst, R. D. *Comp. Organomet. Chem.* **1982**, *3*, 192.
(50) Streitwieser, Jr., A.; Müller-Westerhoff, U. *J. Am. Chem. Soc.* **1968**, *90*, 7364.
(51) Zalkin, A.; Raymond, K. N. *J. Am. Chem. Soc.* **1969**, *91*, 5667.
(52) Streitwieser, A., Jr.; Yoshida, N. *J. Am. Chem. Soc.* **1969**, *91*, 7528.
(53) Hodgson, K. O.; Raymond, K. N. *Inorg. Chem.* **1972**, *11*, 3030.
(54) Dolg, M.; Fulde, P.; Küchle, W.; Neumann, C.; Stoll, H. *J. Chem. Phys.* **1991**, *94*, 3011.
(55) Dolg, M.; Fulde, P.; Stoll, H.; Preuss, H.; Chang, A.; Pitzer, R. M. *Chem. Phys.* **1995**, *195*, 71.
(56) Liu, W.; Dolg, M.; Fulde, P. *J. Chem. Phys.* **1997**, *107*, 3584.
(57) Greco, A.; Cesca, S.; Bertolini, G. *J. Organomet. Chem.* **1976**, *113*, 321.
(58) (a) DeKock, C. W.; Ely, S. R.; Hopkins, T. E.; Brault, M. A. *Inorg. Chem.* **1978**, *17*, 625. (b) Ely, S. R.; Hopkins, T. E.; DeKock, C. W. *J. Am. Chem. Soc.* **1976**, *98*, 1624.
(59) Odas, E.; Kortan, A. R.; Kopylov, N.; Ramirez, A. P.; Siegrist, T.; Rabe, K. M.; Bair, H. E.; Schuppler, S.; Citrin, P. H. *Nature* **1995**, *375*, 126.
(60) Hoshino, K.; Kurikawa, T.; Takeda, H.; Nakajima, A.; Kaya, K. *J. Phys. Chem.* **1995**, *99*, 3053.
(61) Kurikawa, T.; Hirano, M.; Takeda, H.; Yagi, K.; Hoshino, K.; Nakajima, A.; Kaya, K. *J. Phys. Chem.* **1995**, *99*, 16248.
(62) Kurikawa, T.; Takeda, H.; Nakajima, A.; Kaya, K. *Z. Phys. D* **1997**, *40*, 65.
(63) Judai, K.; Hirano, M.; Kawamata, H.; Yabushita, S.; Nakajima, A.; Kaya, K. *Chem. Phys. Lett.* **1997**, *270*, 23.
(64) Hirano, M.; Judai, K.; Nakajima, A.; Kaya, K. *J. Phys. Chem. A* **1997**, *101*, 4893.
(65) Yasuike, T.; Nakajima, A.; Yabushita, S.; Kaya, K. *J. Phys. Chem. A* **1997**, *101*, 5360.
(66) Nakajima, A.; Nagao, S.; Takeda, H.; Kurikawa, T.; Kaya, K. *J. Chem. Phys.* **1997**, *107*, 6491.
(67) Kurikawa, T.; Nagao, S.; Miyajima, K.; Nakajima, A.; Kaya, K. *J. Phys. Chem. A* **1998**, *102*, 1743.
(68) Nagao, S.; Kurikawa, T.; Miyajima, K.; Nakajima, A.; Kaya, K. *J. Phys. Chem. A* **1998**, *102*, 4495.
(69) Kurikawa, T.; Negishi, Y.; Hayakawa, F.; Nagao, S.; Miyajima, K.; Nakajima, A.; Kaya, K. *J. Am. Chem. Soc.* **1998**, *120*, 11766.
(70) Yasuike, T.; Yabushita, S. *J. Phys. Chem. A* **1999**, *103*, 4533.
(71) Nagao, S.; Kurikawa, T.; Miyajima, K.; Nakajima, A.; Kaya, K. Submitted to *J. Phys. Chem. A.*
(72) Geusic, M. E.; Morse, M. D.; O'Brien, S. C.; Smalley, R. E. *Rev. Sci. Instrum.* **1985**, *56*, 2123.
(73) Harberland, H. *Clusters of Atoms and Molecules*; Springer-Verlag: Berlin, 1994; p 230.
(74) Hotop, H.; Lineberger, W. C. *J. Phys. Chem. Ref. Data* **1975**, *4*, 539.
(75) Esaulov, V. A. *Ann. Phys. Fr.* **1986**, *11*, 493.
(76) Weis, P.; Kemper, P. R.; Bowers, M. T. *J. Phys. Chem. A* **1997**, *101*, 8207.
(77) Moore, C. E. Analysis of Optical Spectra. NSRDS-NBS 34; National Bureau of Standards: Washington, DC, 1971. (b) Weast, R. C. *Handbook of Chemistry and Physics*; CRC Press: Boca Raton, FL, 1980; Vol. 61, p E-69. (c) Robinson, J. W. *Handbook of Spectroscopy*; CRC Press: Boca Raton, FL, 1974; Vol. 1, p 257.
(78) Parks, E. K.; Klots, T. D.; Winter, B. J.; Riley, S. J. *J. Chem. Phys.* **1993**, *99*, 5831.
(79) Guo, B. C.; Kerns, K. P.; Castleman, A. W., Jr. *J. Chem. Phys.* **1992**, *96*, 8177.
(80) Fayet, P.; McGlinchey, M. J.; Wöste, L. H. *J. Am. Chem. Soc.*, **1987**, *109*, 1733.
(81) Vajda, S.; Wolf, S.; Leisner, T.; Busolt, U.; Wöste, L. H.; Wales, D. J. *J. Chem. Phys.* **1997**, *107*, 3492.
(82) Yang, S.; Knickelbein, M. B. *J. Chem. Phys.* **1990**, *93*, 1533.
(83) Zakin, M. R.; Cox, D. M.; Brickman, R. O.; Kaldor, A. *J. Phys. Chem.* **1989**, *93*, 6823.
(84) Irion, M. P.; Schnabel, P.; Selinger, A. *Ber. Bunsen-Ges. Phys. Chem.* **1990**, *94*, 1291.
(85) Tast, F.; Malinowski, N.; Billas, I. M. L.; Heinebrodt, M.; Branz, W.; Martin, T. P. *J. Chem. Phys.* **1997**, *107*, 6980.
(86) Cotton, F. A.; Wilkinson, G. *Advanced Inorganic Chemistry*, 5th ed.; John Wiley & Sons: New York, 1988.
(87) Sievers, M. R.; Armentrout, P. B. *J. Phys. Chem.* **1995**, *99*, 8135.
(88) Meyer, F.; Armentrout, P. B. *Mol. Phys.* **1996**, *88*, 187.
(89) Andrews, M. P.; Mattar, S. M.; Ozin, G. A. *J. Phys. Chem.* **1986**, *90*, 1037.
(90) Goldberg, N.; Hoffmann, R. *Inorg. Chem.* **1996**, *35*, 4369.
(91) Rogers, J. R.; Marynick, D. S. *Chem. Phys. Lett.* **1993**, *205*, 197.
(92) Jiao, Q.; Huang, Y.; Lee, S. A.; Gord, J. R.; Freiser, B. S. *J. Am. Chem. Soc.* **1992**, *114*, 2726.
(93) Kinsley, S. A.; Streitwieser, A., Jr.; Zalkin, A. *Organometallics* **1985**, *4*, 52.
(94) Kinsley, S. A.; Streitwieser, A., Jr.; Zalkin, A. *Acta Crystallogr.* **1986**, *C42*, 1092.
(95) Evans, W. J.; Shreeve, J. L.; Ziller, J. W. *Polyhedron* **1995**, *14*, 2945.
(96) Streitwieser, Jr., A.; Kinsley, S. A.; Rigsbee, J. T. *J. Am. Chem. Soc.* **1985**, *107*, 7786.
(97) Clark, J. P.; Green, J. C. *J. Chem. Soc., Dalton Trans.* **1977**, 505.
(98) (a) Dewar, M. J. S.; Gleicher, G. J. *J. Am. Chem. Soc.* **1965**, *87*, 685. (b) Fray, G. I.; Saxton, R. G. *The Chemistry of Cyclooctatetraene and its Derivatives;* Cambridge University Press: Cambridge, 1978.
(99) Nagao, S.; Negishi, Y.; Kato, A.; Nakamura, Y.; Nakajima, A.; Kaya, K. *J. Phys. Chem. A* **1999**, *103*, 8909.